YALE
PEABODY
MUSEUM

P.O. BOX 208118 | NEW HAVEN CT 06520-8118 USA | PEABODY.YALE. EDU

JOURNAL OF MARINE RESEARCH

The *Journal of Marine Research,* one of the oldest journals in American marine science, published important peer-reviewed original research on a broad array of topics in physical, biological, and chemical oceanography vital to the academic oceanographic community in the long and rich tradition of the Sears Foundation for Marine Research at Yale University.

An archive of all issues from 1937 to 2021 (Volume 1–79) are available through EliScholar, a digital platform for scholarly publishing provided by Yale University Library at https://elischolar.library.yale.edu/.

Requests for permission to clear rights for use of this content should be directed to the authors, their estates, or other representatives. The *Journal of Marine Research* has no contact information beyond the affiliations listed in the published articles. We ask that you provide attribution to the *Journal of Marine Research*.

Yale University provides access to these materials for educational and research purposes only. Copyright or other proprietary rights to content contained in this document may be held by individuals or entities other than, or in addition to, Yale University. You are solely responsible for determining the ownership of the copyright, and for obtaining permission for your intended use. Yale University makes no warranty that your distribution, reproduction, or other use of these materials will not infringe the rights of third parties.

This work is licensed under a Creative Commons Attribution-NonCommercial-ShareAlike 4.0 International License.
https://creativecommons.org/licenses/by-nc-sa/4.0/

Journal of Marine Research, 54, 867–913, 1996

Analysis of the North Atlantic climatologies using a combined OGCM/adjoint approach

by Lisan Yu[1] and Paola Malanotte-Rizzoli[1]

ABSTRACT

An exact adjoint for the full-scale Bryan-Cox primitive equation model is applied to assimilate the North Atlantic climatologies. The inverse calculation aims at searching a steady state oceanic general circulation consistent with observations, by controlling the model input parameters (such as the initial states and the upper thermal and haline boundary conditions). Two climatological hydrographies (Levitus (1982) and Fukumori and Wunsch (1991)) are used for the assimilation. This enables the examination of the sensitivity of the assimilated results to data quality. In addition, the consistency between the climatological hydrography and fluxes is discussed by examining the fits between the optimally estimated surface fluxes and the fluxes calculated by Oberhuber (1988). The efforts made in the study are directed toward assessing the effectiveness of the combined OGCM/adjoint approach in estimating the state of the ocean from climatologies and identifying the associated problems.

The major findings of the study include: (1) The results show that the full OGCM dynamics substantially helps the model in better simulating the frontal structure of the Gulf Stream system and the large-scale features of the velocity field, thus demonstrating the advantage of the full OGCM and its exact adjoint. (2) The study finds that the optimized temperature field has a systematic error structure in the vertical—*the upper ocean is cooler and the deep ocean is warmer* compared to the climatology. Our analysis indicates that the cool surface layer is a correction imposed by the optimization to reduce large data misfits in the deep ocean due to the deep warming. This deep warming is an outcome of using the steady state assumption, the annual mean climatology and the relaxation boundary condition at the model northern boundary. The annual mean hydrography has a surface water warmer than the observed winter surface water, and a deep ocean whose properties are determined by the surface water at high latitudes. Due to the imposed model northern boundary condition, the modeled deep waters are formed through the artificial sinking of surface waters with annual-mean temperature in the relaxation zone. This process leads to a warm deep ocean and large model-data discrepancies in the vast deep layer. In order to reduce the misfits as required by the optimal procedure, the surface layer which is the source for the modeled deep water needs to be cooler. The strong and deep vertical mixing formed in the model provides the means for an effective cooling. The results further show that the surface cooling is stronger for the experiment assimilating the Fukumori and Wunsch hydrography because this climatology has an even warmer surface water due to the use of the summer-dominated data source. (3) The experiments assimilating the Levitus hydrography illustrate two anomalous features, one is a strong zonally integrated upwelling in the midlatitude and the other a very noisy flux estimation. The analysis shows that both features are

1. Center for Meteorology and Physical Oceanography, Department of Earth, Atmospheric, and Planetary Sciences, Massachusetts Institute of Technology, Cambridge, Massachusetts, 02139 U.S.A.

induced by the smeared representation of the Gulf Stream frontal structure in the Levitus hydrography, which indicates that data quality is one of the important factors in obtaining satisfactory results from the assimilation. (4) Although the requirements for a global minimum are only partially satisfied, the experiments show that, comparing with the Levitus hydrography, the Fukumori and Wunsch hydrography is dynamically more compatible with the Oberhuber climatological fluxes.

1. Introduction

Combining model with observations, or data assimilation, has proved to be a powerful method in estimating unobserved quantities from observables, filling in information in data-poor regions and generating assimilated oceanic data sets with physical consistency. Lately, data assimilation has drawn much attention from oceanographers due to practical reasons. One is that recent developments in remote sensing techniques and their applications to observing oceanographic fields have opened an era of data revolution. The tremendous amount of data enables oceanographers to examine oceanic signals that are linked to climate variability on many time scales. Yet, diagnosing and understanding such an observed, complicated ocean system as a response to the observed atmospheric forcing require a sophisticated ocean general circulation model (OGCM). Today's OGCMs are equipped with complex dynamics and run with eddy-resolving resolution and realistic geometry. Nevertheless their capability in realistically simulating the three-dimensional ocean circulation is limited not only by the poorly known model inputs (such as the surface momentum, heat and fresh water fluxes and eddy-mixing coefficients) but also by the insufficient representation of interior physics. As a result, the oceanic data assimilation being pursued lays much emphasis on testing model physics and improving numerical models.

Among many available data assimilation techniques, the adjoint method is perhaps the most promising and practical approach in combining complex ocean general circulation models with large data sets. The adjoint method is originated from the variational method and the optimal control theory, where the name "adjoint" stems from the fact that this method requires the solution of the adjoint equations of the linearized model equations. As has been described in the papers by Le Dimet and Talagrand (1986) and Thacker and Long (1988), this powerful inverse method works in a fashion that model unknowns are estimated by fitting model to data. More specifically, an optimization problem in an adjoint approach is formulated such that the finding of optimal unknown model parameters is made through minimizing a cost function or distance between observations and model counterparts over the time interval considered. The minimization is sought by using a gradient-based algorithm in which the value of the gradient of the cost function with respect to the model unknowns is supplied by the integration of the adjoint model. By incorporating the physics of the problem (e.g., model dynamics and/or any physical or statistical constraints to the solution) into the definition of the cost function, this method essentially gives no limitation to the characteristics of data as long as the data contain the information desired by the model.

There is growing interest in the oceanographic society in applying the adjoint technique

to oceanic general circulation models. Tziperman *et al.* (1992a,b) made the first attempt with a simplified (using the planetary geostrophic approximation of the momentum dynamics) Bryan-Cox Ocean Model (Bryan, 1969; Cox, 1984) for analyzing North Atlantic oceanographic observations in the dynamical framework of a steady state solution. Marotzke and Wunsch (1993) re-experimented the work of Tziperman *et al.* with the same simplified OGCM but improved the integration strategy. Their application was motivated by the finding of Marotzke (1992) that a longer time integration is needed in order to obtain a compromise solution between data constraints and steadiness constraints. In addition, Bergamasco *et al.* (1993) found consistent steady state solutions using an adjoint technique for the full-scale OGCM in studying the steady circulation of the Eastern Mediterranean. More recently, Schiller and Willebrand (1995) described an approximate adjoint to the Bryan-Cox model which is actually the adjoint equations for only the temperature and salinity fields. Though computationally attractive, the approximate adjoint model is not able to assimilate the velocity observations and optimize the wind field.

In this study an exact adjoint model to the full Bryan-Cox primitive equation model (Yu and Malanotte-Rizzoli, 1995) is used. Compared with the previous studies which usually used simplified dynamics (Tziperman *et al.,* 1992a,b; Marotzke, 1992; and Marotzke and Wunsch, 1993) or simplified adjoints (Schiller, 1995; Schiller and Willebrand, 1995), this adjoint OGCM has the full dynamics which can resolve better some important dynamical features, such as the Gulf Stream and fronts. Moreover, the exact adjoint formulation in this study allows the model to be used for more general applications, such as estimating the air-sea momentum fluxes. The adjoint code is constructed from the original prototype developed at the Atlantic Oceanographic and Meterological Laboratory (Long *et al.,* 1989). The inverse calculation aims at searching a steady state oceanic general circulation in the North Atlantic consistent with climatologies, by controlling the model input parameters of the initial states and the upper thermal and haline boundary conditions.

Three specific objectives are carried out in the study. The first and foremost objective is to examine the influence of data on assimilated results by comparing the experiments using the climatologies from Levitus (1982) and from Fukumori and Wunsch (1991). As is known, differences in hydrographic structures could lead to different model dynamical responses, which in turn can be used to measure the dynamical information in data. In this study the response of the model to changes brought by the assimilation is analyzed through examining properties of the transport of horizontal gyres, meridional overturning and northward heat transport, air-sea fluxes of heat, and evaporation minus precipitation.

The second objective is to study the determination of model unknowns from the climatological hydrographic data and/or flux data. The surface heat and fresh water fluxes represent the model thermal and haline upper boundary conditions. From the thermodynamic point of view, they can be determined solely from the hydrographic data if data are sufficient. Therefore, the addition of the climatological flux data (Oberhuber, 1988) to the optimization raises a question: are the fluxes determined from the hydrographic data

consistent with the flux atlas? Experiments are designed to explore the dynamical coupling between the hydrographic and flux data.

The third objective is to study the impact of the model on the propagation of data information. The full-scale Bryan-Cox primitive equation model is expected to provide more complete dynamical descriptions of the ocean circulation than the simplified OGCMs. The effectiveness of using this model for assimilation is assessed through comparisons with previous studies. On the other hand, the parameterization schemes are not perfect and numerical models have errors. These errors can lead to systematic error corrections by the assimilation, which in turn induces unrealistic adjustment to the model. Therefore, attempts are made to identify the model errors through vigorous model-data comparisons and analyses.

The plan of the paper is as follows. In Section 2, the formulation of the adjoint procedure for the problem is discussed. The description of data and experiment design is given in Section 3. The assimilated results are compared and analyzed in Section 4. Section 5 concludes the paper. A brief description of the Bryan-Cox primitive equation model is included in the Appendix.

2. Formulation of the adjoint procedure

The adjoint optimization procedure consists of three major elements: a physical model, an adjoint model of the linearized physical model, and a minimization algorithm. The Bryan-Cox primitive equation model is the physical model in our study of the large-scale oceanic circulation in the North Atlantic. The technical details have been described in documents by Bryan (1969) and Cox (1984). Only a brief description of the model and features linked to the adjoint formulation are given here (see Appendix). The methodology of the adjoint approach has also been discussed by many researchers. The readers are referred to the studies by Le Dimet and Talagrand (1986) and Thacker and Long (1988) for theoretical guidance.

a. Model configuration

The model domain covers the North Atlantic ocean from 10N to 65N and from 100W to 0, with a realistic bathymetry (Fig. 1). The resolution is 1.2° in longitude and 2° in latitude with 22 levels in the vertical. These levels are distributed at the depths of 25, 75, 150, 250, 350, 450, 550, 650, 750, 850, 950, 1100, 1350, 1650, 2000, 2400, 2800, 3250, 3750, 4250, 4750 and 5250 m. The island of Cuba is cut off. Near the northern and southern walls, a narrow buffer zone is included in which the model properties (T, S) are damped toward their climatological values on a time scale of 30 days. This effectively permits a flux of heat and salt through the side boundaries in spite of the insulating boundary condition (see Eq. A7 in the Appendix). A similar buffer zone is also inserted near the Mediterranean Sea outflow region (in the depths between 900 and 2400 m) with a time scale of 360 days. The parameterization of subgrid mixing is chosen as $A_h = 10^5\ m^2\ s^{-1}$, $A_v = 10^{-3}\ m^2\ s^{-1}$, $K_h = 10^3\ m^2\ s^{-1}$, and $K_v = 3 \times 10^{-5}\ m^2\ s^{-1}$. A synchronous scheme is applied for the model integration with the timestep of one hour for both momentum and tracer equations.

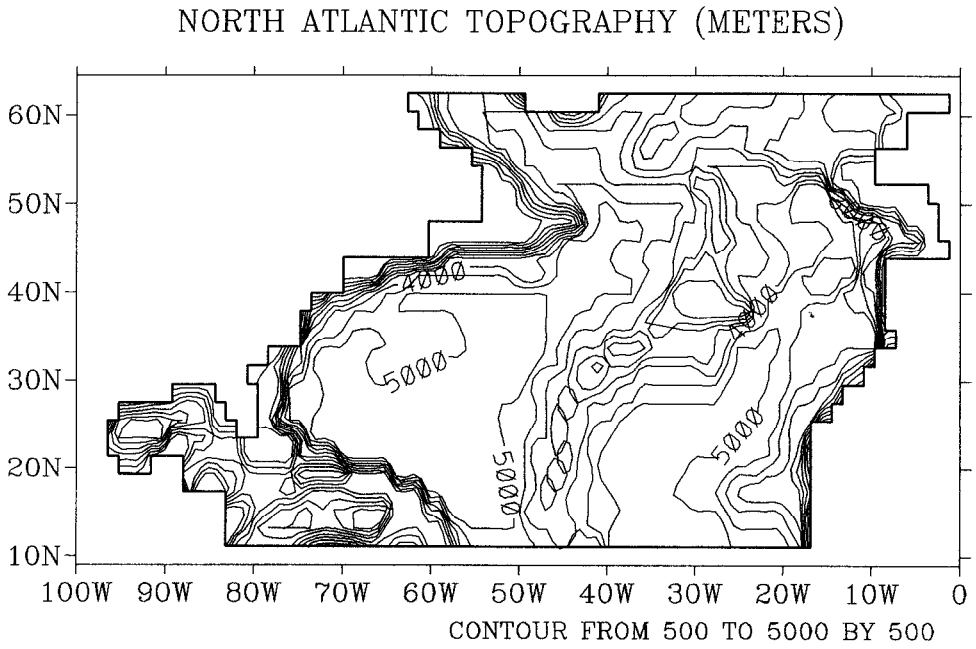

Figure 1. The model bathymetry (CI = 500 m).

b. Formulating the adjoint procedure using a primitive equation model

In adjoint calculations, the model performance is evaluated by comparing the modeled fields with the chosen observations; their mismatches are formulated into a cost function. The cost structure represents the objective of optimization and the cost value is used as a criterion in searching optimal values of the model inputs to make the model close to data to the degree of data accuracy. In complying with the principle of the adjoint approach, we formulate a cost function using a least-squares formalism, which is

$$\begin{aligned}\mathcal{J} = &\underbrace{\frac{1}{2}\sum_{i,j,k}[W_k^T(T_{ijk}^{n=N_T} - \hat{T}_{ijk})^2 + W_k^S(S_{ijk}^{n=N_T} - \hat{S}_{ijk})^2]}_{\text{I}} \\ &+ \frac{1}{2}\sum_{i,j,k}[W_k^{ST}(T_{ijk}^{n=N_T} - T_{ijk}^{n=0}) + W_k^{SS}(S_{ijk}^{n=N_T} - S_{ijk}^{n=0})^2 \\ &+ \underbrace{W_k^{S\mathbf{u}}(\mathbf{u}_{ijk}^{n=N_T} - \mathbf{u}_{ijk}^{n=0})^2]}_{\text{II}} \\ &+ \underbrace{\frac{1}{2}\sum_{i,j}[W^{QT}(Q_{Tij} - \hat{Q}_{Tij})^2 + W^{Qs}(Q_{Sij} - \hat{Q}_{Sij})^2]}_{\text{III}}\end{aligned} \tag{1}$$

where T represents the temperature, S the salinity, $\mathbf{u}$ the the horizontal velocity vector, Q_T the surface heat flux, and Q_S the surface fresh water flux. For convenience, we stay in the discrete space where the OGCM is formulated. The data values are denoted by the caret ($\hat{}$), the model final states by the index ($n = N_T$) where N_T is the total model integration time, and the initial states by the index ($n = 0$).

The weight function coefficients W_k^T, etc., reflect the relative precision of observations. For simplicity, we assume that they vary with depth only. The weights for groups (I) and (III) are given as

$$W_k^T = \frac{\langle \sigma_{Tk} \rangle^{-2}}{N_3}, \qquad W_k^S = \frac{\langle \sigma_{Sk} \rangle^{-2}}{N_3} \tag{2}$$

$$W^{Q_T} = \frac{\langle \sigma_{Q_T} \rangle^{-2}}{N_2}, \qquad W^{Q_S} = \frac{\langle \sigma_{Q_S} \rangle^{-2}}{N_2} \tag{3}$$

where $\langle \sigma_{Tk} \rangle$ and $\langle \sigma_{Sk} \rangle$ are the horizontal means of the hydrographic data error at level k; $\langle \sigma_{Q_T} \rangle$ and $\langle \sigma_{Q_S} \rangle$ the means of the flux data error (see Section 3 for further discussion). N_3 is the total number of the model grid-points, and N_2 the total number of the horizontal grid-points. The weights in the group (II) are determined following the definition by Marotzke and Wunsch (1993)

$$W_k^{Sm} = \frac{\langle \sigma_{mk} \rangle^{-2}}{N_3} \left(\frac{\Gamma}{N_T} \right)^2, \qquad \text{where } m = T, S, \mathbf{u} \tag{4}$$

where Γ is equivalent to the adjustment timescale of the processes one wants to equilibrate. We specify Γ to be 10 years.

The cost function in (1) is formulated in the same way as the one appearing in the paper by Marotzke and Wunsch (1993). It is different from the one used by Tziperman *et al.* (1992a,b) only in the sense that the model is allowed to step in time for a certain period instead of a single time-level. The terms in the group (I) are misfits between the modeled and the climatological temperature and salinity fields. The temporal derivatives, represented by the terms in the group (II), are penalized as the differences between the modeled final and initial states of the integration period. The group (III) includes the terms which measure the departure of estimated controls Q_T and Q_S from their climatological values.

The goal of the optimization is to find the optimal values for the control $\hat{\mathscr{X}}_{ijk}^{n=0}$, Q_{Tij} and Q_{Sij} such that the corresponding model solution $\hat{\mathscr{X}}_{ijk}^{n=N_T}$ obtained from the model equations (Eq. A20 in Appendix) reaches a steady state and meanwhile the model state $T_{ijk}^{n=N_T}$ and $S_{ijk}^{n=N_T}$ close to the chosen climatological state. Mathematically this problem belongs to the class of the constrained optimization and can be solved by enforcing the equations (A20) with Lagrange multipliers, λ. A Lagrangian function is then formulated as follows

$$\mathscr{L} = \mathscr{T} + \sum_{ijkn} \lambda_{ijk}^n [\hat{\mathscr{X}}_{ijk}^n - \mathscr{F}_n(\hat{\mathscr{X}}_{ijk}^{n-1}, Q_{Tij}, Q_{Sij})]. \tag{5}$$

Here the model equations are used as the "strong" constraint by the definition of Sasaki (1970). By doing so, the problem of finding the minimal points of $\mathcal{J}$ constrained by the model equations (A20) becomes the problem of finding the stationary points of $\mathcal{L}$. The condition of stationary points requires that the first order variation of $\mathcal{L}$ with respect to all the variables vanish. This gives the following set of equations after some simple algebra

$$\frac{\partial \mathcal{L}}{\partial \lambda_{ijk}^{n}} = 0 \Rightarrow \mathcal{X}_{ijk}^{n} = \mathcal{F}_n(\mathcal{X}_{ijk}^{n-1}, Q_{Tij}, Q_{Sij}) \qquad \text{(dynamical model (A20))} \tag{6}$$

$$\frac{\partial \mathcal{L}}{\lambda . \mathcal{X}_{ijk}^{n}} = 0 \Rightarrow \lambda_{ijk}^{n} = \left[\frac{\partial \mathcal{F}_{n+1}}{\partial \mathcal{X}_{ijk}^{n}}\right]^{T} \lambda_{ijk}^{n+1} - \frac{\partial \mathcal{J}}{\partial \mathcal{X}_{ijk}^{n}} \qquad \text{(Adjoint model)} \tag{7}$$

$$\frac{\partial \mathcal{L}}{\partial Q_{mij}} = 0 \Rightarrow \frac{\partial \mathcal{J}}{\partial Q_{mij}} + \sum_{n=1}^{N_T} \left[\frac{\partial \mathcal{F}_n}{\partial Q_{mij}}\right]^{T} \lambda_{ijk}^{n} = 0 \qquad \text{where } m = T, S \tag{8}$$

$$\frac{\partial \mathcal{L}}{\partial \mathcal{X}_{ijk}^{n=0}} = 0 \Rightarrow \frac{\partial \mathcal{J}}{\partial \mathcal{X}_{ijk}^{n=0}} + \lambda_{ijk}^{n=0} = 0. \tag{9}$$

The resulting equations represent the primitive equation model (Eq. 6), the adjoint model (Eq. 7), the gradient of $\mathcal{J}$ with respect to the controls of Q_{Tij} and Q_{Sij} (Eq. 8), and the gradient of $\mathcal{J}$ with respect to the model initial states (Eq. 9). Eqs (8) and (9) are satisfied only when the optimal solution of controls $\mathcal{X}_{ijk}^{n=0}$, Q_{Tij} and Q_{Sij} are obtained. During the minimization, the nonzero left-hand sides of these two equations provide the gradient information of the cost function with respect to the controls.

The adjoint procedure is an iterative process which produces a better approximation to the optimal solution with each iteration. The procedure starts with choosing best guess values for the controls for integrating the dynamical model. The time history of the model fields $\mathcal{X}_{ijk}^{n}$ is saved for calculating the misfit fields. The adjoint model is integrated backward in time with the initial condition $\lambda_{ijk}^{n=N_T+1} = 0$. By using the information carried by the Lagrange multipliers, the gradients can be calculated and then used by a minimization algorithm (e.g., the conjugate gradient method (Navon and Legler, 1987)) to construct a new search direction $\mathbf{d}^{\text{new}}$. The values of the controls are updated according to

$$\mathcal{C}^{\text{new}} = \mathcal{C}^{\text{old}} + \beta \mathbf{d}^{\text{new}} \qquad \text{where } \mathcal{C} = \mathcal{X}_{ijk}^{n=0}, Q_{ij}^{T}, Q_{ij}^{S} \tag{10}$$

where β is the size for the correction; it is determined by a process called "the line search," in which at least one additional forward model run is performed to find an optimal value for β. There are some convergence criteria. If they are satisfied, the procedure is stopped; otherwise, the procedure is repeated with the updated control values. One can see that one complete cycle of the variational adjoint procedure demands minimal three model runs of comparable complexity. For a sophisticated model like the OGCM we are using, hundreds of iterations are performed to find a minimum.

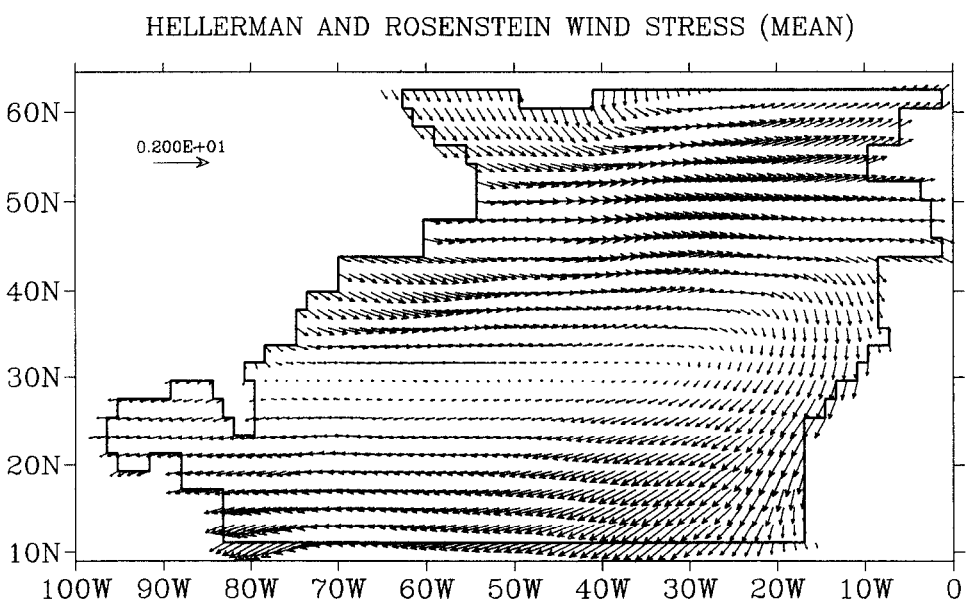

Figure 2. The Hellerman and Rosenstein annual-mean wind stress.

3. The database and the experiment design

The study uses the annually averaged climatological data for searching a steady model state. The wind data (Fig. 2) are taken from the Hellerman and Rosenstein (1983) climatology. The surface heat and fresh water (defined as evaporation minus precipitation) flux data (Fig. 3) are taken from the Oberhuber (1988) atlas. The wind stress field remains unchanged during the optimization. Two climatological hydrographies are used for the assimilation. One is compiled by Fukumori and Wunsch (1991) (hereafter referred to FW91) and the other is taken from the Levitus (1982) atlas. Note that the FW91 climatology extends from 80W to 10W in longitude and from 10N to 60N in latitude. The potential temperature fields of these two data sets at the depth of 25 m are depicted in Figure 4. Although both climatologies exhibit a similar large-scale hydrographic structure of the North Atlantic Ocean, differences are visible.

These differences can be traced back to the use of different data sources and data processing procedures during the map compilation. The FW91 climatology was constructed from the data acquired by CTDs between 1981 and 1985. The data processing procedure used vertical Empirical Orthogonal Functions (EOFs) (Fukumori *et al.*, 1991; Fukumori and Wunsch, 1991). The first six EOF modes are then combined with the horizontal objective mapping to form the gridded climatology (see Appendix A in the paper by Marotzke and Wunsch (1993)). In contrast, the Levitus climatology was based on the data collected from the hydrographic stations as well as the mechanical and expendable bathythermography survey from the early 1990s to the mid 1970s. The data processing procedure included an isobaric averaging scheme and a horizontal objective mapping.

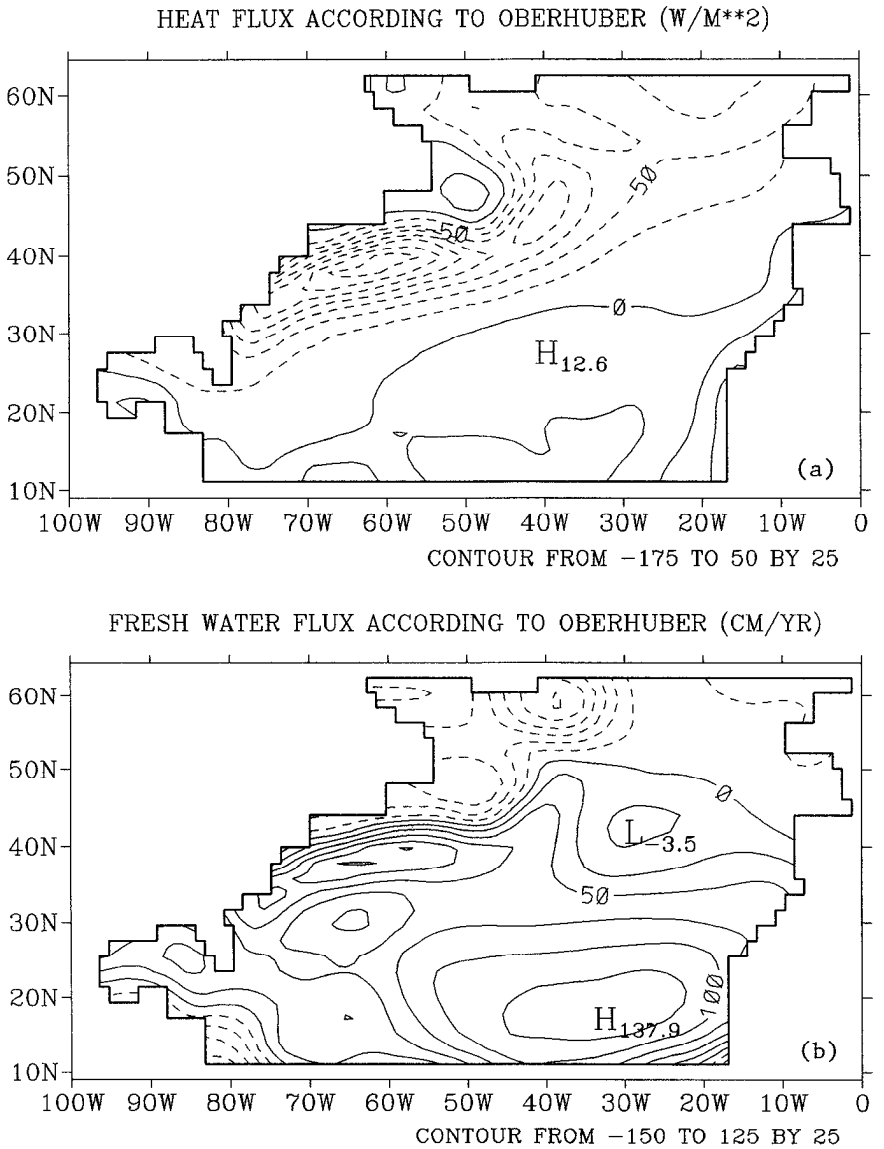

Figure 3. The Oberhuber annual-mean (a) surface heat flux (CI = 25 W/m^2) and (b) evaporation minus precipitation flux (CI = 25 cm/year).

However, studies have shown (e.g., Lozier *et al.*, 1994) that this climatological averaging not only resulted in weak gradients in frontal areas but created anomalous water masses with temperature-salinity characteristics dissimilar to the surrounding water (Lozier *et al.*, 1994). The impacts of this averaged data set on assimilated results are examined in later sections.

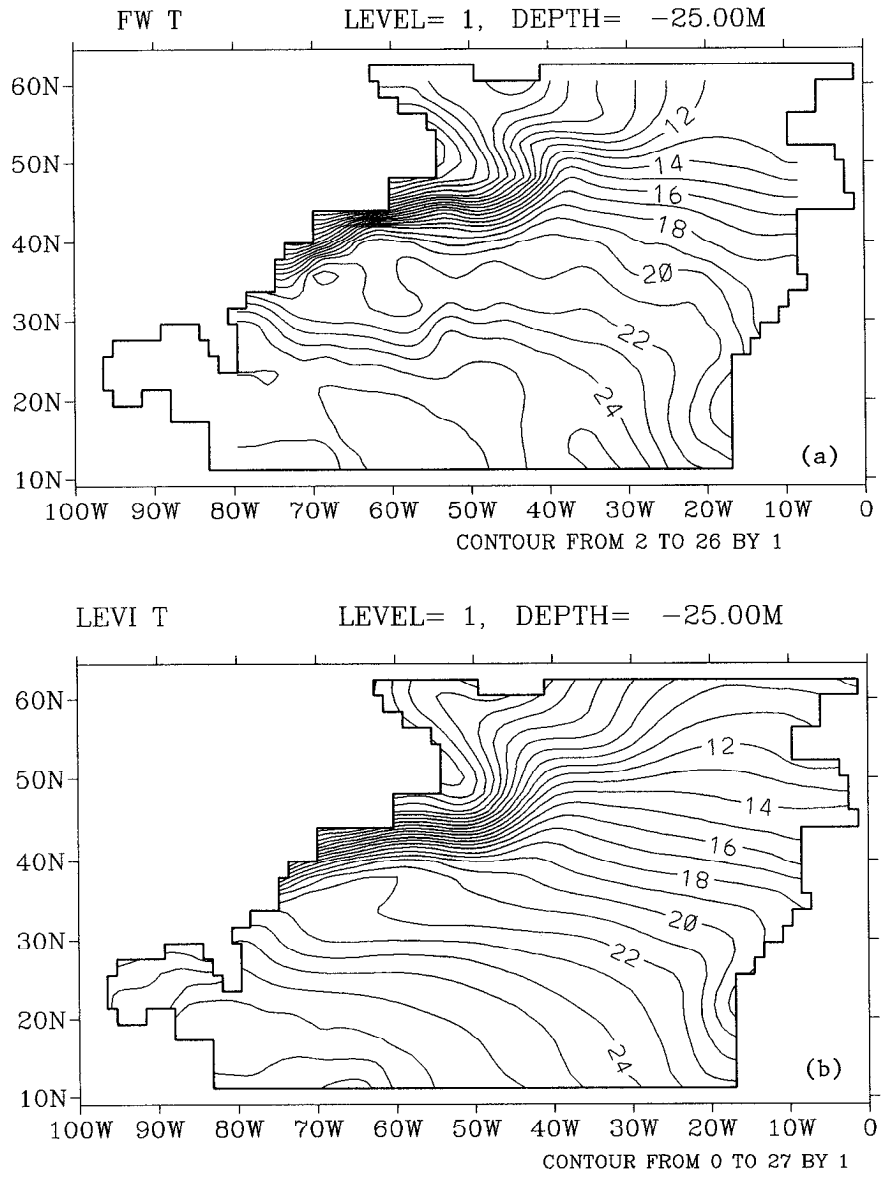

Figure 4. The potential temperature at the sea surface. (a) Fukumori and Wunsch climatology and (b) Levitus climatology (CI = 1°C).

For simplicity all the data sets have been linearly interpolated onto the model grid to make the model-data comparisons easy. Information about the data error distribution is needed to compute the weights in the cost function (1). The errors for the FW91 hydrographic fields (Fig. 5) were obtained from the objective analysis scheme. These error

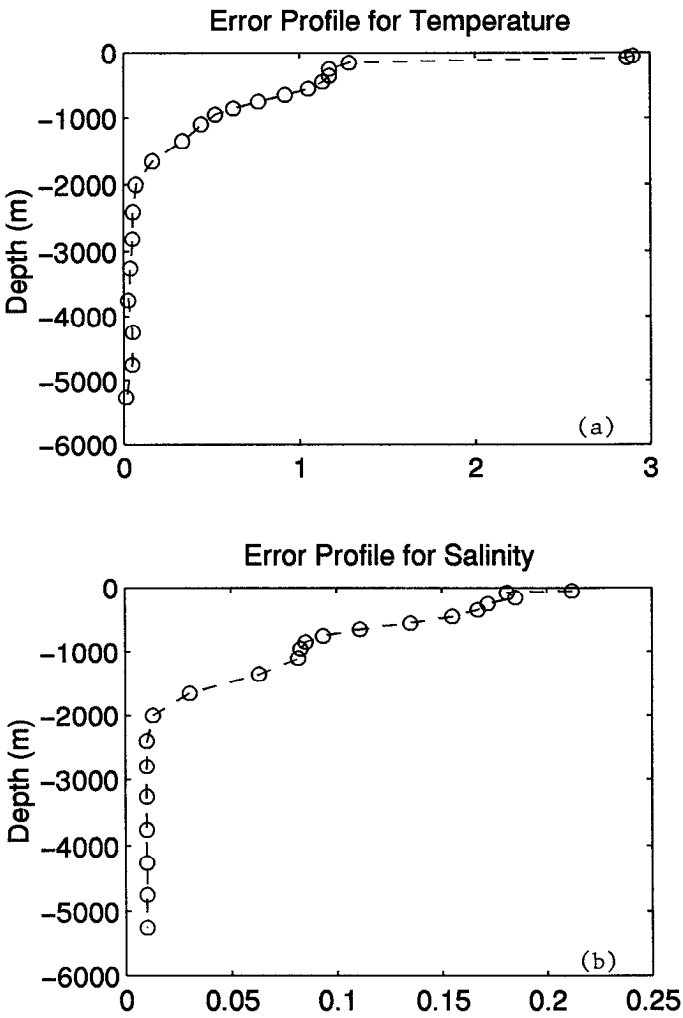

Figure 5. The error profile for (a) the potential temperature and (b) the salinity.

estimates are also applied to the Levitus climatology. Note that in Figure 5 the values in the upper two layers have been readjusted to adapt the unsampled seasonal variability. The errors for the heat and fresh water fluxes from the Oberhuber climatology are not known. We therefore simply choose a uniform value of 75 W/m^2 for the heat flux and 50 cm/year for the fresh water flux. Compared to existing documents (e.g. Weare *et al.*, 1981), the error bar for the heat flux is slightly larger, since an additional consideration about the model uncertainty is imposed. The errors for current velocities are estimated to be 2.5 cm/sec at the surface down to 0.2 cm/sec near the bottom.

Four experiments (Table 1) are conducted. Exps. I and II are designed to determine the surface heat and fresh water fluxes directly from the hydrographic observations. The

Table 1. Experiment Design.

Experiment	Data	Cost function	First guess for the model initials
I	FW91	data misfit + steady penalty	final state of 250-day spin-up starting from the FW91 hydrography
II	Levitus	same as Exp. I	final state of 250-day spin-up starting from the Levitus hydrography
III	FW91	data misfit + steady penalty + flux penalty	same as Exp. I
IV	Levitus	same as Exp. III	same as Exp. II

minimization searches for optimal estimates of the model surface flux conditions and the initial conditions so that the circulation constructed is steady and consistent with the climatological hydrography. Note that the estimations of surface fluxes are not restricted by any constraints in these cases. The experiments assume very large flux uncertainty (i.e., $W^{Q_T} \rightarrow 0$ and $W^{Q_S} \rightarrow 0$) and allow large departures of the estimated flux fields from their corresponding climatological values. Exps. III and IV examine the consistency between the climatological hydrography and fluxes. In these two experiments, the minimization requires that not only the model steady state be consistent with the climatological hydrography, but the estimated surface fluxes be close to the climatological fluxes.

In all the experiments, the guess values for the surface heat and fresh water fluxes are chosen to be Oberhuber fluxes. The guess values for the ocean state are taken from the final state of the 250-day spin-up of the Bryan-Cox OGCM. The spin-up runs are initialized with the annual mean temperature and salinity from either the FW91 climatology or the Levitus climatology depending upon the type of data used in the assimilation. During the spin-ups, the Hellerman and Rosenstein (1983) wind stress is used to drive the momentum equations, and the Han (1984) heat flux formulation and the surface restoring scheme are employed in the temperature and the salinity integrations respectively.

4. Results and analysis

a. Variations of the cost function: Has the minimum been reached?

The variations of the cost function and the norm of the gradients with the number of iterations are shown in Figure 6. During each experiment, the iterative process is terminated when the following two criteria are satisfied: (1) the current initialized L_2 norm of the cost gradients is of $O(10^{-4})$ and (2) the change of the cost value during the last 15 iterations is of $O(10^{-2})$. These two conditions define a computational steady solution of the adjoint procedure. The total number of iterations performed ranges from 190 (Exp. II) to 210 (Exp. IV). We choose an integration time of 180 days at the beginning of the minimization and increase it to 250 days and 500 days whenever an insufficient reduction in the cost value occurs (e.g., the integration time for Exp. I is altered at iteration 75 and again at iteration 100, where sharp jumps are clearly seen in the plot of the norm of the gradients (Fig. 6b)). The use of the tunable integration length is mainly based on the

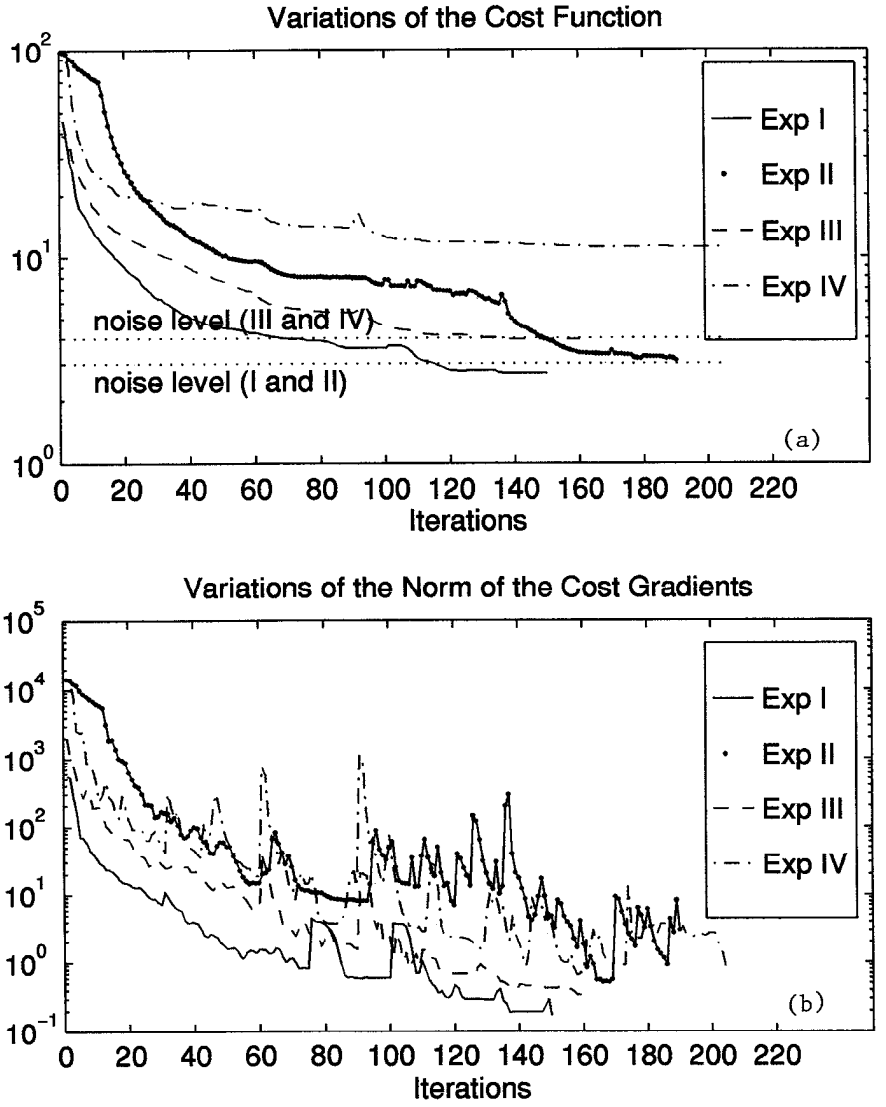

Figure 6. The variations of (a) the cost function and (b) the norm of the gradient during the optimization.

consideration of the computational efficiency. However the monotonous increase of the integration time will not always guarantee an effective cost reduction. For example, Schiller and Willebrand (1995) found that the optimal integration time in their experiments was between $O(10^2)$ and $O(10^3)$ days.

Theoretically, for a well-conditioned system, a minimum is obtained when a compromise between data and steadiness constraints is achieved. A compromised solution

Table 2. The variations of the Cost Function.

Experiment	J_{begin}	J_{end}	T_{misfit}	S_{misfit}	T_{steady}	S_{steady}	U_{steady}	V_{steady}	$Q_{T,misfit}$	$Q_{S,misfit}$
1	38.98	2.67	0.65	0.39	0.73	0.71	0.10	0.08		
2	97.58	3.10	0.32	0.16	1.38	0.85	0.17	0.22		
3	45.65	3.94	0.66	0.40	0.98	0.92	0.24	0.24	0.25	0.24
4	97.57	11.1	0.32	0.16	1.61	0.91	0.33	1.10	2.61	4.10

represents a cost state at which all sets of constraints are equally large. In addition, it requires that each cost individual term is of the order of the pre-assumed error estimates, which means each cost value should be of the magnitude of 0.5. Figure 6 shows that Exps. I, II and III have the similar cost behavior during the optimization, that is, the convergent rate slows down after 60–80 iterations and the cost value is at the noise level when the iterative process is terminated. In contrast, Exp. IV has a faster cost reduction during the first 20 iterations and the change of the cost value thereafter is insignificant. At the end of the optimization its total cost value is much higher than the pre-assumed noise level. Obviously, the optimality is not achieved in Exp. IV.

Table 2 lists the total and individual cost values for all experiments. One sees that Exps. I and II which have the same cost formulation obtain a normalized total cost value of roughly 3 at the end of the optimizations. The data misfit terms have roughly the same order of magnitude as the steady state residuals. One also notices that Exps. III and IV have converged to different cost values, one is at 3.9 (Exp. III) and the other at 11.1 (Exp. IV). It seems that appending the flux penalties to the cost function can lead to distinct responses for a model which assimilates Levitus hydrographic climatology. This is further indicated by the individual cost values at the end of the minimization (Table 2). In Exp. III, each cost component contributes roughly equally to make up the total cost value, while in Exp. IV the hydrographic data misfits are not compatible with their steadiness residuals and the flux misfits are dominant over the rest terms. By examining the cost behavior in all of the four experiments, one can say that, except Exp. IV, all the other three experiments basically satisfy the global requirement for a minimum.

In the next section we examine the optimal solutions in the model dynamic framework. We shall examine issues concerning the sensitivity of the model to climatology and the consistency between the flux and hydrographic climatologies. The effects of the cost formulation on the optimization are investigated and the acceptability of the solutions from the oceanographic point of view is discussed.

b. Results from Exps. I and II

i. Hydrographic fields. Figure 7 display the FW91 climatological sea surface temperature (SST), the SST field obtained at the optimal solution in Exp. I and the residual fields. The extensive surface cooling at the model's northwestern corner is inherited from the input first guess field, which is taken from the final state of the 250-day spin-up (note that the spin-up run is initialized by the same climatology used in the assimilation). The spin-up

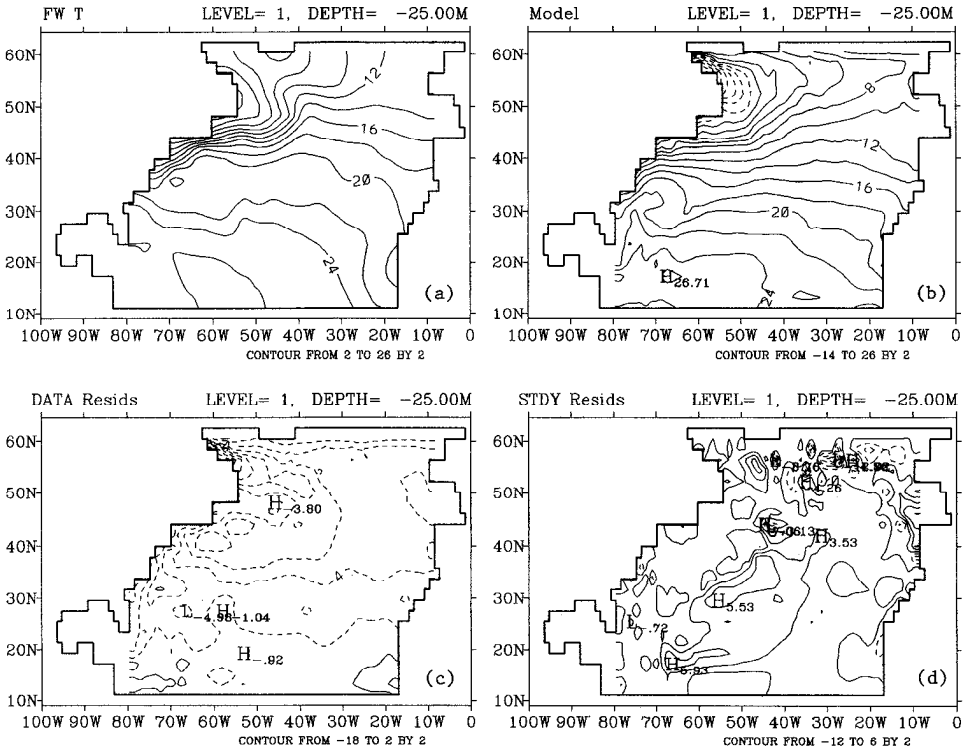

Figure 7. Results from Exp. I. (a) the potential temperature from the Fukumori and Wunsch climatology; (2) the optimized potential temperature; (c) the data residuals ($T_{ijk}^{n=N_T} - \hat{T}_{ijk}$); and (d) the steadiness residuals ($T_{ijk}^{n=N_T} - T_{ijk}^{n=0}$) × (10 years/$N_T$), where $T_{ijk}^{n=N_T}$ denotes the temperature at the final state and $T_{ijk}^{n=0}$ the initial temperature). All shown at the surface level (CI = 2°C).

model specifies the upper thermal boundary condition according to the Han (1984) heat flux formula. This flux parameterization scheme computes the heat flux as a linear function of the difference between the modeled SST and a prescribed effective atmospheric temperature. Due to the missing physics (e.g., the mechanism of sea-ice formation) in the model, cold atmospheric temperatures at higher latitudes in the Han's restoring scheme directly produce cold SSTs underneath. The adjoint assimilation, which strongly depends on the first-guess field due to the model's nonlinearity, seems only to reduce the strength of the cooling but not to correct it. This localized cooling structure is also shown in the other three experiments.

From Figure 7 one observes that the adjoint calculations have reproduced well the large-scale SST structure of the climatology. More importantly, the calculations have produced some dynamical features absent or distorted in the climatology, such as the front north of the Florida Straits. Compared to the studies which used the simplified OGCM (Marotzke and Wunsch, 1993), the features in the SST field (e.g., the Gulf Stream and the fronts) are simulated better with the full OGCM in use. However the optimized SST is, in

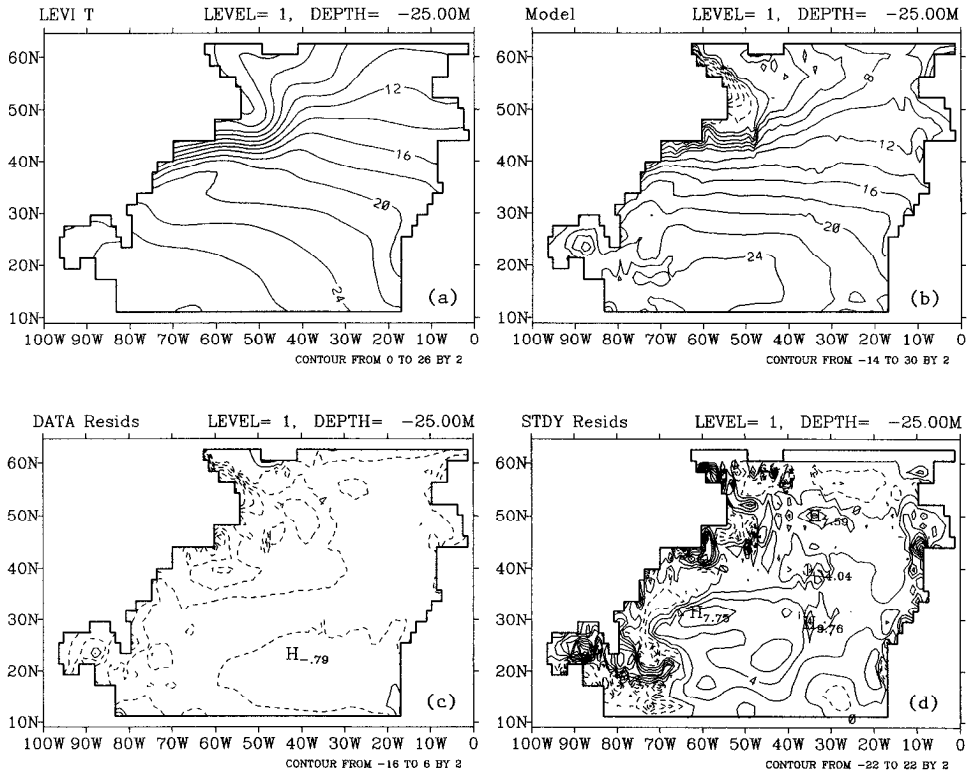

Figure 8. As in Figure 7 but for Exp. II.

general, cooler than the climatology. For example, the 20°C isotherm in the model is about 10° southward compared with the data. If examining the surface temperature data residual field, one notices that the modeled field is systematically cooler than the observed field and the maximum cooling is of 8°C near the western boundary. That the model produces a cooler sea surface is common to all experiments—it is observed in an experiment which assimilates the Levitus climatology (Fig. 8). The systematic cooling pattern seems to be contradictory to what has been assumed when using a diagonal weighting matrix in (2). The appearance of the large-scale systematic misfit pattern, rather than a random noisy one, suggests a deficiency in either data or model physics. Or as indicated by Sirkes and Tziperman (1995), an insufficient representation of the surface thermal boundary condition might also contribute to the misfit as well.

The systematic surface cooling has also appeared in the studies of Tziperman *et al.* (1992b), Marotzke and Wunsch (1993), and Schiller (1995). Marotzke and Wunsch (1993) attributed the cooling to the use of the steady assumption which excludes the seasonal variations in the calculations. Meanwhile, Tziperman and Bryan (1993) suggested that the cooling might result from using the flux boundary condition which decouples the SST

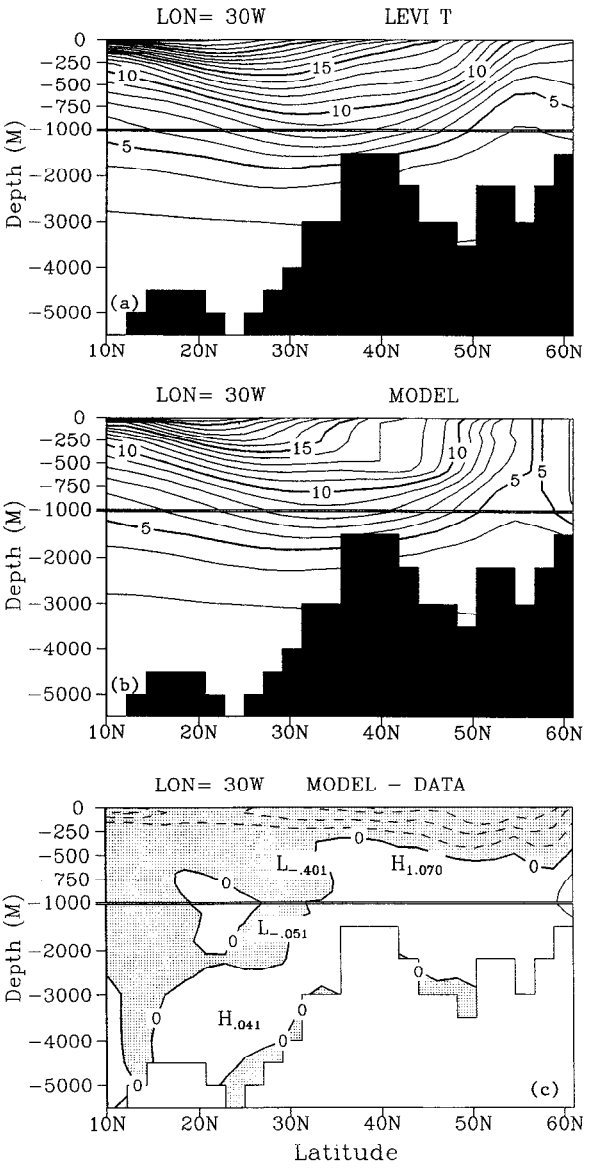

Figure 9. The meridional temperature fields along 30W from (a) the Levitus climatology; (b) Exp. II; and (c) the difference between (b) and (a) (CI = 1°C).

changes with the changes in the air-sea fluxes. Here we are going to explore this issue from the viewpoints of the lease-squares formalism and the model dynamics.

The meridional temperature fields along 30W display that the Levitus climatological field (Fig. 9a) has a strong stratification even at higher latitudes; while the optimized field from Exp. II (Fig. 9b) has a much weaker stratification in general and strong active

convections at higher latitudes. Figure 9c, which is the difference between these two temperature fields, reveals that the cooling is basically confined in the upper 500 m but a warming appears in the vast deep ocean. Analysis of other sections indicates that this is a basin-wide phenomenon—the modeled temperature is *underestimated in the upper ocean and overestimated in the deep ocean.*

We believe that the appearance of this systematic error structure in the vertical is due to the combined effects of using the steady state assumption, the annually averaged hydrography and the relaxation boundary condition at the model's northern boundary. The annual mean hydrography has a surface water warmer than the observed winter surface water and a deep ocean whose properties are determined by the surface water at high latitudes. Since the model domain is limited to 65N, a rigid wall is imposed and a narrow buffer zone is inserted to relax the modeled temperature and salinity toward the climatological values. By doing so, the modeled deep waters are formed through the artificial sinking process in the buffer zone, and the deep water characteristics are therefore determined by the properties of the surface water in the sinking region. Without seasonal cycles, the deep water is produced from sinking the surface water with the annual mean temperature. This leads to a warmer deep ocean and large model-data discrepancies in the vast deep layer. In order to reduce this misfit as required by the optimal procedure, the model's deep water source, i.e., the surface layer, has to be made cooler. Therefore, the systematic surface cooling compensates for the deep warming and is the outcome of the least-squares requirement for an optimal model-data fitting in the three-dimensional space. Strong and deep vertical mixing is formed (Fig. 9b) to provide the mechanism for an effective cooling. It is suggested that a better simulation of the 3-D hydrography requires at least the inclusion of the seasonal cycle. We are now in the progress of assimilating seasonal climatological data.

The degree of the surface correction depends on how much of the surface cooling is necessary to minimize the overall data misfits. From the plot of the temperature differences between Levitus and FW91 climatologies (Fig. 10a), one sees that the upper ocean of the FW91 climatology is much warmer, though the deep water has a similar temperature to that of the Levitus climatology. The warmer surface water in the FW91 climatology is due to the use of the summer-dominated data source (see Table 1 of Fukumori and Wunsch, 1991). When using the FW91 hydrography for the assimilation (Exp. I), it is found that the optimized surface water is about 5°C cooler than the climatology (Fig. 10b)—the surface cooling is stronger than that in Exp. II which assimilates the Levitus hydrography (see Fig. 9c).

Compared to the temperature fields, the optimized surface salinity fields strikingly resemble the climatological fields in the large-scale structure and the magnitude for both Exp. I and II (Figs. 11 and 12). The plots of the model-data difference (Figs. 11c and 12c) show that, though there is a small region along the western boundary where the misfits are larger than two standard deviations, the misfits elsewhere are within the prespecified noise level (0.21 ppt for the surface salinity). The meridional salinity fields along 50W (Fig. 13) also display general agreements between the optimized and the climatological fields over

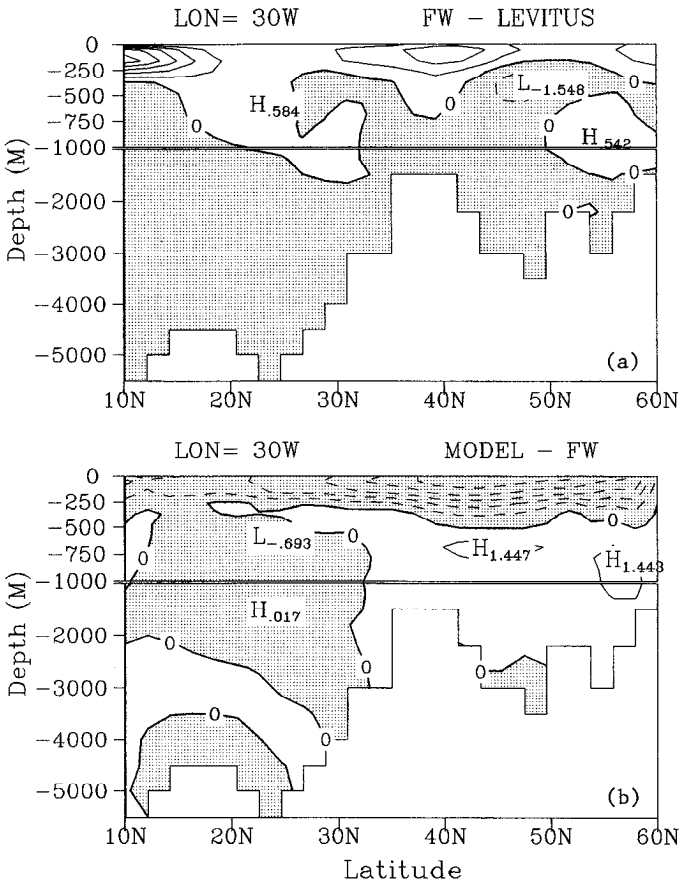

Figure 10. The meridional temperature differences along 30W (a) between the Levitus climatology and the Fukumori and Wunsch climatology; and (b) between Exp. I and the Fukumori and Wunsch climatology (CI = 1°C).

the whole section. The only noticeable difference is that the model has a deeper vertical mixing in the region between 40 and 45N, apparently due to the same mechanism operating in the temperature fields.

The hydrographic fields, both observed and optimized from Exp. I, and their residual fields at 1100 m are displayed in Figures 14 and 15. The plots of data residual fields show that the modeled Mediterranean water outflow is colder and fresher than the data indicate. It seems that the model is insufficient to generate the strong front described by the climatology, even though a narrow buffer zone (see the description in Section 2a) is inserted around 36N along the eastern boundary. One should remember that, though the buffer zone plays a role in forcing the model properties (T, S) toward their observed values, the physical condition of the Mediterranean outflow is not defined. Compared with the results from Marotzke and Wunsch (1993), it is clear that the inclusion of the sponge layer

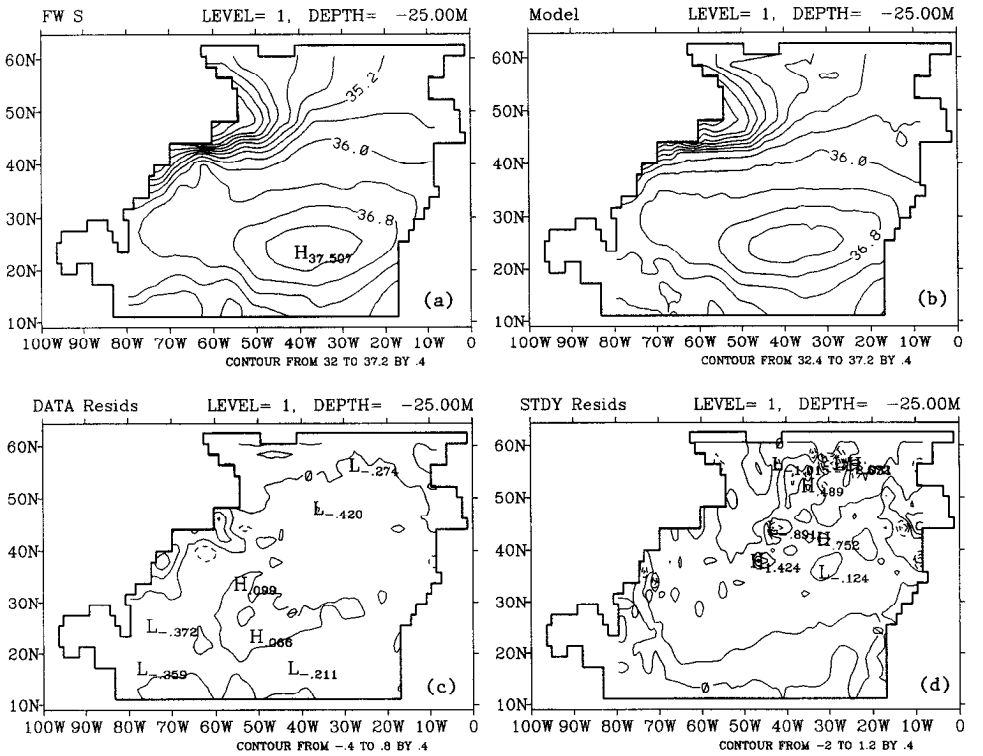

Figure 11. Results from Exp. I. (a) the salinity from the Fukumori and Wunsch climatology; (b) the optimized salinity; (c) the data residuals ($S_{ijk}^{n=N_T} - \hat{S}_{ijk}$); and (d) the steadiness residuals ($S_{ijk}^{n=N_T} - S_{ijk}^{n=0}$) $\times$ (10 years/N_T), where $S_{ijk}^{n=N_T}$ denotes the salinity at the final state and $S_{ijk}^{n=0}$ the salinity at the initial state). All shown at the surface level (CI = .4 ppt).

outside of the Mediterranean Sea does not resolve better the frontal structure. The fact that the missing physics results in the weaker Mediterranean tongue is illustrated more clearly in the steadiness residual plots. Perceiving a systematic discrepancy, the adjoint procedure tries to push the model state close to data by setting a warmer and saltier Mediterranean outflow at the initial state. This feature could not be sustained by the present model physics however, and not surprisingly the model signals a cooling and freshening trend (Figs. 14d and 15d). For Exp. II, the residual fields at the depth of 1100 m have the similar structure to those of Exp. I and so only temperature residuals are shown (Fig. 16). Compared to Exp. I, the temperature field seems to have a better agreement with the data considering that the Levitus climatology has a weaker front. However, the steady residual field has a larger temporal drift especially in the northern domain.

In general, the data and steadiness residual fields, either at the surface or at the depth of 1100 m, have shown a systematic misfit pattern especially for the temperature. As is stated above, this feature does not fully satisfy the requirements for a global minimum.

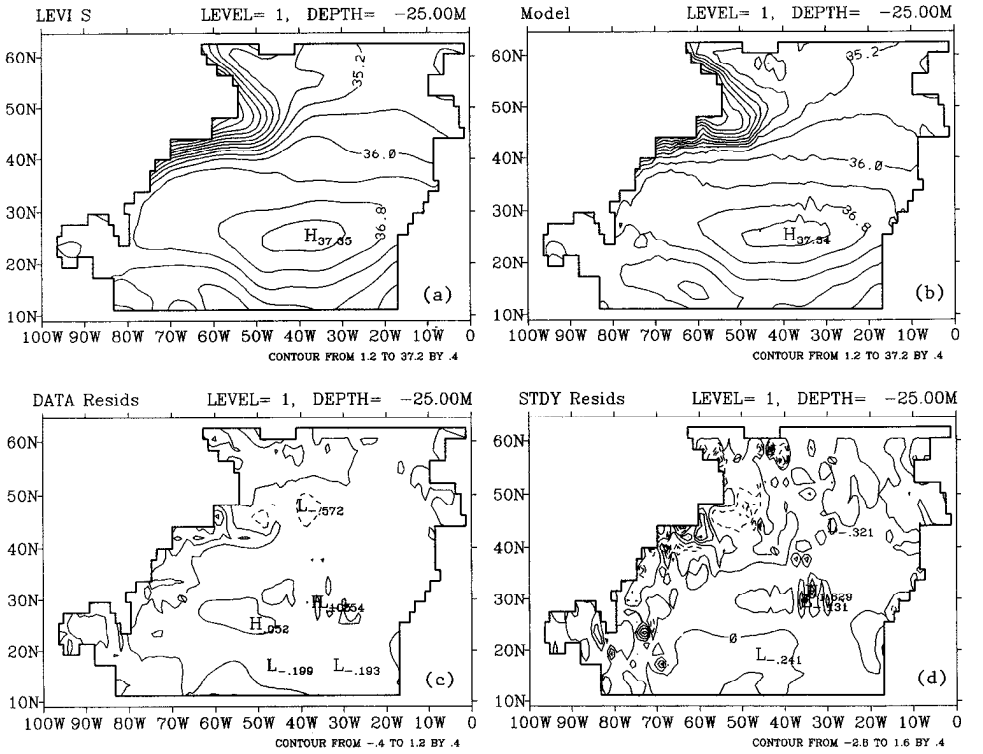

Figure 12. As in Figure 11 but for Exp. II.

Nevertheless, the overall magnitudes of data and steadiness residuals in Exp. I are within the prescribed errors rather than in Exp. II, in which the steadiness residuals larger than two standard deviations appear in many areas. It seems that, within the current dynamical framework, the FW91 hydrography is more compatible than the Levitus hydrography.

ii. Mean circulation. Velocity observations are not available for the study. During the optimization, the adjustments to the velocity fields are made through both the steadiness demands and the indirect coupling to the hydrographic data via the pressure gradients.

Maps of the horizontal velocity fields at the optimal solution at depths of 25 m, 1100 m and 2400 m from Exp. I are shown in Figure 17. Features of the large-scale circulation are clearly seen. For example, the surface velocity field has the subtropical gyre circulation with a strong western boundary current, and the subpolar gyre circulation with the North Atlantic current. The deeper water circulation (e.g. 2400 m) shows the deep western boundary current (DWBC) flowing southward all the way from the northern boundary to the southern boundary. The velocity fields obtained from Exp. II (Fig. 18) display a similar circulation pattern. However, compared to the classical view of the mean flow pattern, the modeled North Atlantic current in both experiments is rather weak. This is believed to be

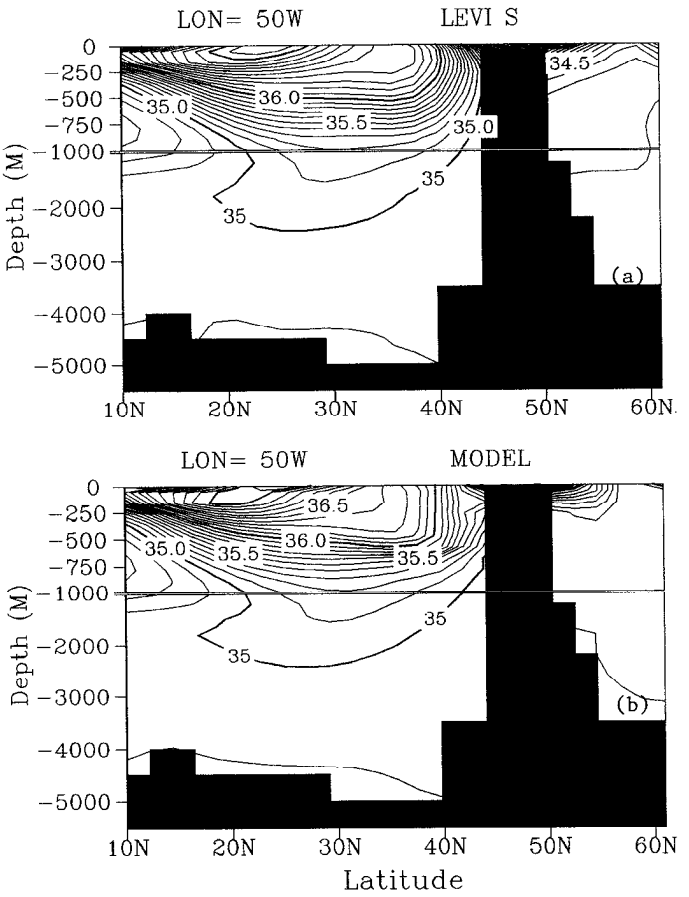

Figure 13. The meridional salinity fields along 50W from (a) the Levitus climatology; and (b) Exp. II.

mainly due to the limitation of the model domain, which is located south of 65N and does not include the Nordic Seas. However, the North Atlantic current system, to some extent, is driven by the surface to deep water conversion at the Nordic Seas.

The barotropic transport stream functions obtained from Exps. I and II are also plotted in Figures 17 and 18. Although the subtropical western boundary transports in these two experiments are similar, the magnitude of the southward transports associated with the subpolar gyre are quite different. The transports of 24 Sv are produced in Exp. II which are twice as strong as those in Exp. I. The difference in the subpolar transports is related to the difference in the latitudinal position of the model's northern boundary in the two experiments. The model domain is cut off at 60N for Exp. I because the FW91 hydrography has no data beyond this latitude, while it extends to 65N for Exp. II.

In general, the mean circulation is simulated better than that in the study of Marotzke

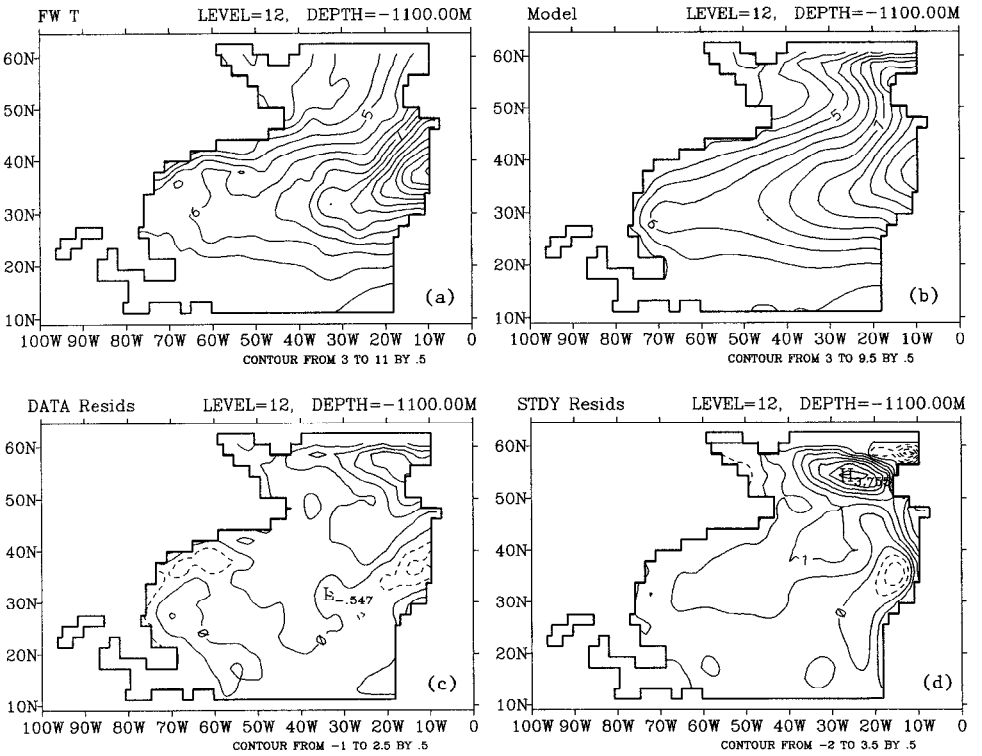

Figure 14. As in Figure 7 but at the depth of 1100 m (CI = 0.5°C).

and Wunsch (1993), in which noisy velocity fields were produced. They attributed the deformity to the use of the Rayleigh friction which does not couple horizontal velocities at neighboring grid points and does not have the same smoothing effects as the Laplacian friction.

iii. Meridional circulation and meridional heat transport. Figure 19 plots the zonally-averaged volume transport stream functions in the meridional-vertical plane. One observes that both experiments have produced a qualitatively similar baroclinic transport structure. For example, shallow overturning cells are developed at the surface as a result of the wind-driven circulation. The major overturning cell is centered around 1000 m depth and its lower branch consists of two water masses, namely, the southward transport of the North Atlantic Deep Water (NADW) (between 1200 and 3500 m) and the northward spreading of the Antarctic Bottom Water (AABW) (below 3500 m). The strong vertical movements in the northern and southern buffer zones (within 4° of the boundaries) are an artifact of the restoring to *T-S* climatology and do not represent the physical flows. In both experiments, the AABW cell has a northward transport of about 1 Sv; yet the NADW cell is found to be

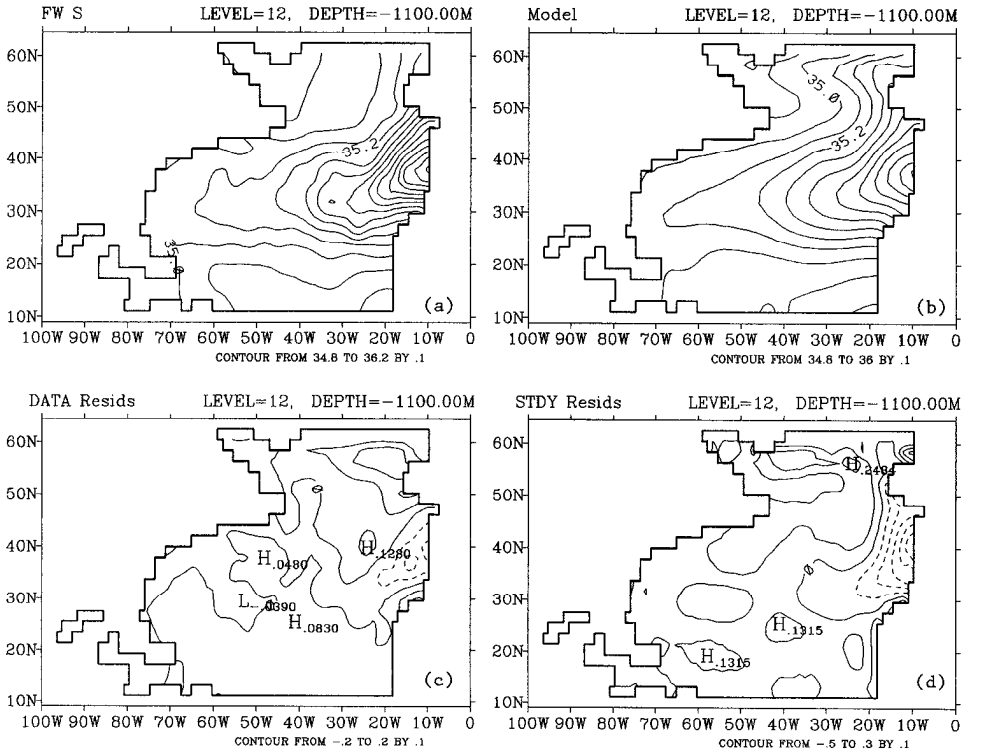

Figure 15. As in Figure 11 but at the depth of 1100 m (CI = 0.1 ppt).

15 Sv in Exp. I and 18 Sv in Exp. II. Obviously the intensity of the NADW cell is sensitive to details of the thermohaline lateral forcing at high latitudes.

Figure 19 also shows that, on the way of southward transporting of the NADW, part of the NADW is upwelled in the midlatitudes between 35 and 45N. The upwelling in Exp. II returns about one third of the NADW production to the surface and reduces the amount of deep water carried to low latitudes to 9 Sv. In contrast, the upwelling in Exp. I is much weaker and the amount of deep water reaching the southern boundary is found to be 11 Sv. Although the NADW cell in Exp. I is 3 Sv smaller than that of Exp. II, 2 Sv more NADW are conveyed to the southern boundary compared to Exp. II. It is clear that the strong upwelling in Exp. II has significantly decreased its NADW transport.

That models of large-scale thermohaline circulations in the Atlantic Ocean exhibit intensive zonally integrated upwelling in midlatitudes has drawn attention to Böning *et al.* (1995). They explained this spurious upwelling as due to the so called "Veronis effect" (Veronis, 1975) by examining the results from a series of the Community Modeling Effort (CME) experiments. The "Veronis effect" is characterized by an anomalous upwelling in the western boundary layer of the subtropical gyre, which results from using a vertical/horizontal mixing parameterization of the temperature and salinity. The mechanism can be

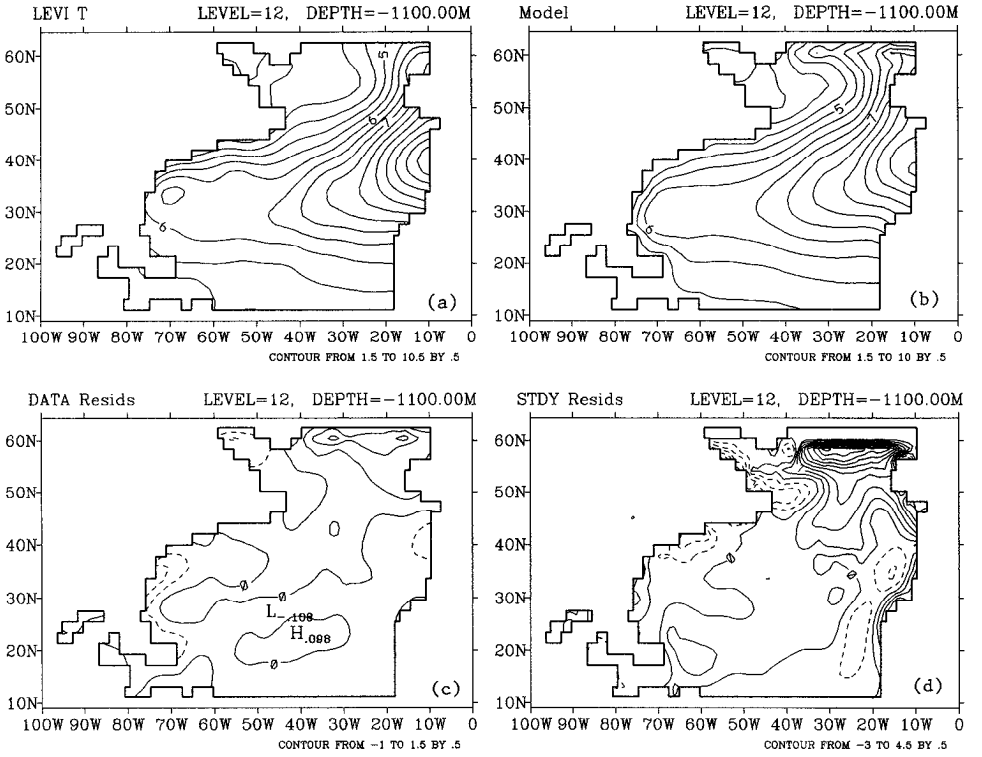

Figure 16. As in Figure 8 but at the depth of 1100 m (CI = 0.5°C).

explained as follows. Along the western boundary, isopycnals outcrop and the horizontal mixing across the Gulf Stream front causes a diapycnal flux of heat and salt. As a result, spurious heat and salt fluxes in regions of steep isopycnal sloping are produced which in turn induce the spurious upwelling of the cold water from the deep ocean (i.e., $w\partial T/\partial z \sim K_h \nabla^2 T$ in the local dynamical balance).

However given the same model configuration and the same numerical model in our study, the upwelling induced by the FW91 hydrography (Exp. I) is much weaker than that by the Levitus hydrography (Exp. II). The zonal temperature field along 40N (not shown) reveals that the frontal structure in the western boundary region is much sharper in the FW91 hydrography than in the Levitus hydrography. If the "Veronis effect" dominated in our case, one should have obtained a stronger upwelling in Exp. I than in Exp. II. Examination of the dynamical balance indicates that the spurious upwelling in Exp. II is largely induced by the *cross-isotherm heat advection* (i.e., $w\partial T/\partial z \sim \mathbf{u} \cdot \nabla_h T$), a feature associated with the distorted front in the Levitus hydrography.

Shown in Figure 20 are the temperature fields at 850 m from the two climatologies. The upwelling occurs near the western boundary at the latitude around 45N. In this region, the FW91 climatology shows clearly the structure of the Gulf Stream and its extension, in

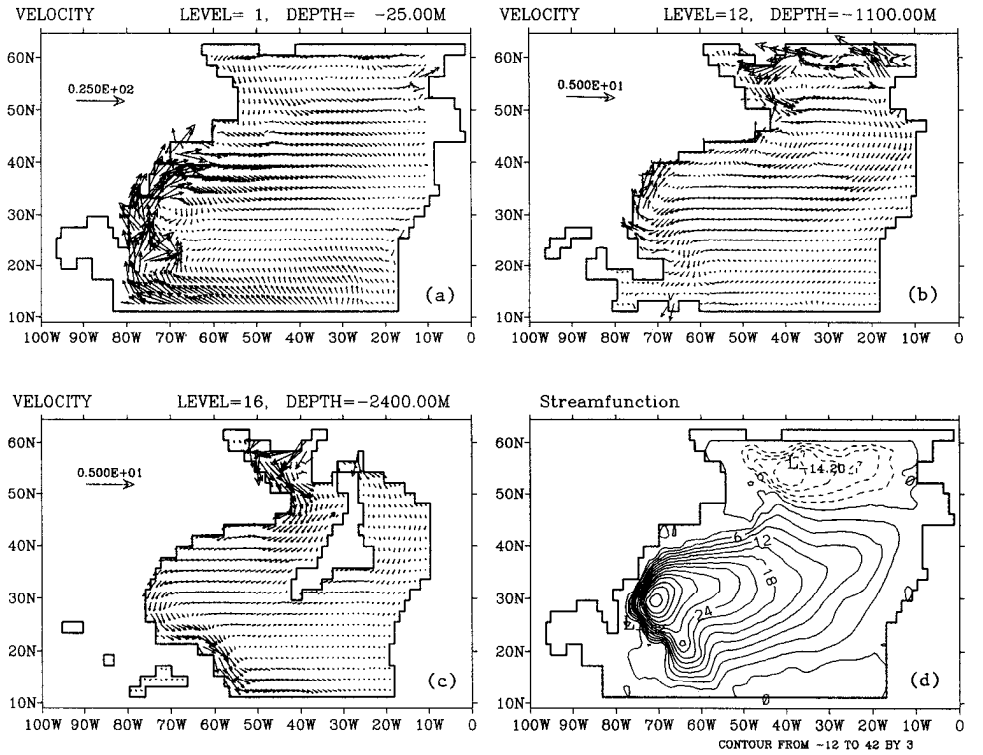

Figure 17. Results from Exp. I. The current velocity at depths of (a) 25 m, (b) 1100 m, and (c) 2400 m. The barotropic stream function (Sv) is shown in (d).

which the isotherms are directed mostly meridionally. In contrast, the isotherms in the Levitus climatology are zonally and uniformly oriented; moreover, the front between 50 and 40W is smeared. Since the upper ocean is wind-driven, the velocity structures in the two experiments are similar. Given that the magnitude of $\mathbf{u} \cdot \nabla_h T$ reflects the degree of the parallelism between the streamline and the isotherm, one can expect that such parallelism is more prevailing in FW91 hydrography. Therefore the flux of $\mathbf{u} \cdot \nabla_h T$ is exaggerated when assimilating the Levitus climatology. To balance it, an enhanced upwelling is required.

The meridional heat transports associated with these two experiments are displayed in Figure 21. Compared to Exp. I (Fig. 21a), the advective heat transport in Exp. II (Fig. 21b) is larger at higher latitudes (north of 32N) and relatively smaller at lower latitudes. In both experiments the diffusive heat transport is small. The advective poleward heat transport in the North Atlantic is mainly determined by the heat transport carried by meridional overturning cells. At higher latitudes, the strength of the heat transport depends on the strength of the NADW cell, which is why Exp. II has a larger heat transport. At lower latitudes, Exp. II has a lower NADW overturning rate and a weaker surface overturning cell, and therefore less heat is transported to the north. Clearly the spurious midlatitude

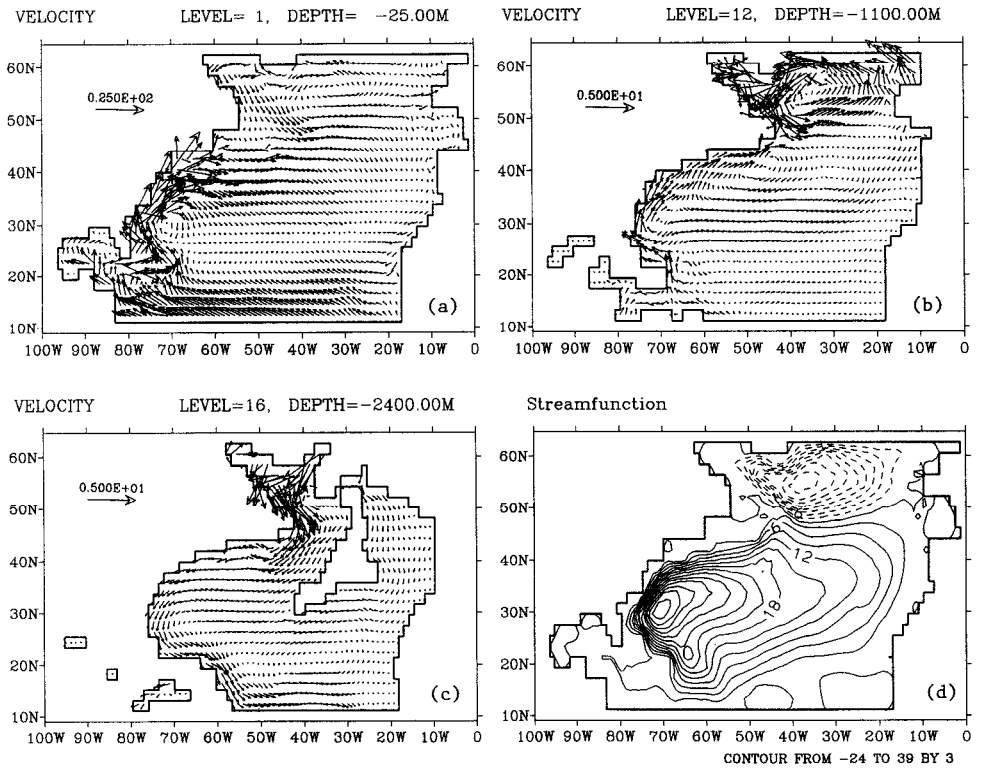

Figure 18. As in Figure 17 but for Exp. II.

upwelling and the corresponding weakening of the overturning rate have significant influences on the latitudinal structure of the meridional heat transport.

Examining the detail of Figure 21c, one obtains a net heat transport of 0.74 Petawatts (1 PW = 10^{15} Watts) in Exp. I and of 0.60 Petawatts in Exp. II at about 25N. These values are much smaller than estimates given by Hall and Bryden (1982) who obtained a transport of 1.2 $\pm$ 0.3 PW at this latitude. Studies have shown that almost all the numerical models are insufficient in predicting the observed net northward heat transport (Holland and Bryan, 1993). Böning *et al.* (1995) pointed out that the spurious midlatitude upwelling might be the major deficiency for models—this seems to be the case for Exp. II. As for Exp. I, we think that the weaker NADW cell is the reason for the weaker poleward heat transport.

iv. Estimated surface heat and fresh water fluxes: Comparisons between Exp. I and the Oberhuber climatology. Figure 22 displays the optimal surface heat and fresh water fluxes computed from Exp. I. Comparing with the Oberhuber climatology (Fig. 3), one observes that these two flux maps are similar with regards to the large-scale flux distribution structure. For example, both heat flux maps show a strong heat release of the ocean to the atmosphere over the Gulf Stream region and at higher latitudes, and also they have a weak

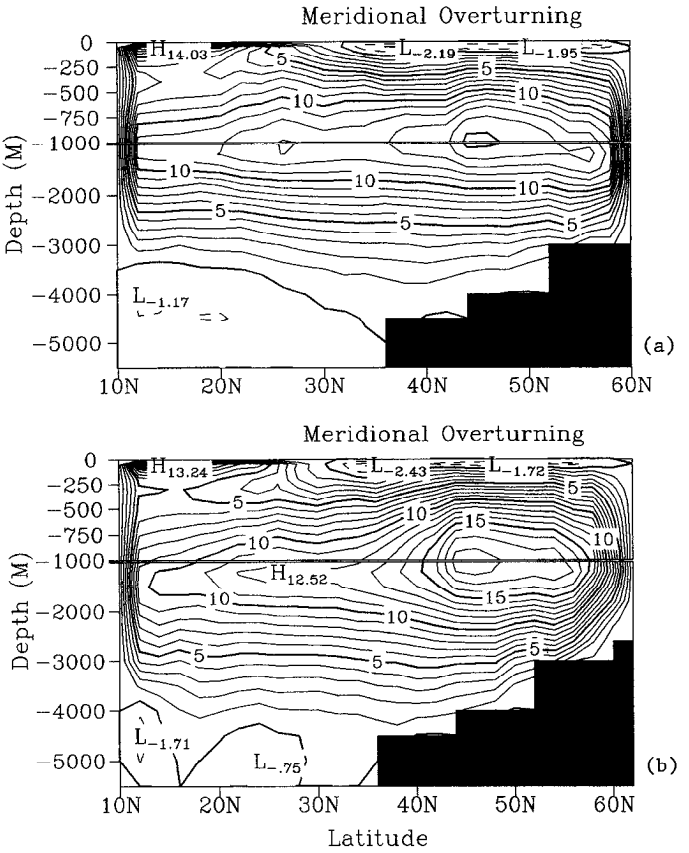

Figure 19. The meridional transport stream function (Sv) obtained from (a) Exp. I and (b) Exp. II (CI = 1 Sv).

air-sea heat flux transfer over the broad area of the central subtropics. Moreover, both fresh water flux estimates predict an excess evaporation in the subtropics and an excess precipitation in the subpolar regions. Nevertheless a major difference exists between the optimal and the Oberhuber fluxes. Near the coast of Newfoundland, the optimal heat flux shows a center of heat uptake of the ocean, in contrast, the climatology has a heat loss center. In the same position, the estimated fresh water flux also shows a center of high evaporation, different from what is shown in the climatological flux. The fluxes estimated by Schiller (1995) displayed the similar localized features.

By virtue of the adjoint calculation, the estimated surface fluxes describe the optimal upper boundary conditions required by the OGCM in obtaining a steady state solution close to the climatology. Analysis of the modeled upper ocean state indicates that the appearance of the localized heating and evaporation is due to the model's insufficiency in simulating the North Atlantic Current. The weak North Atlantic Current in the model

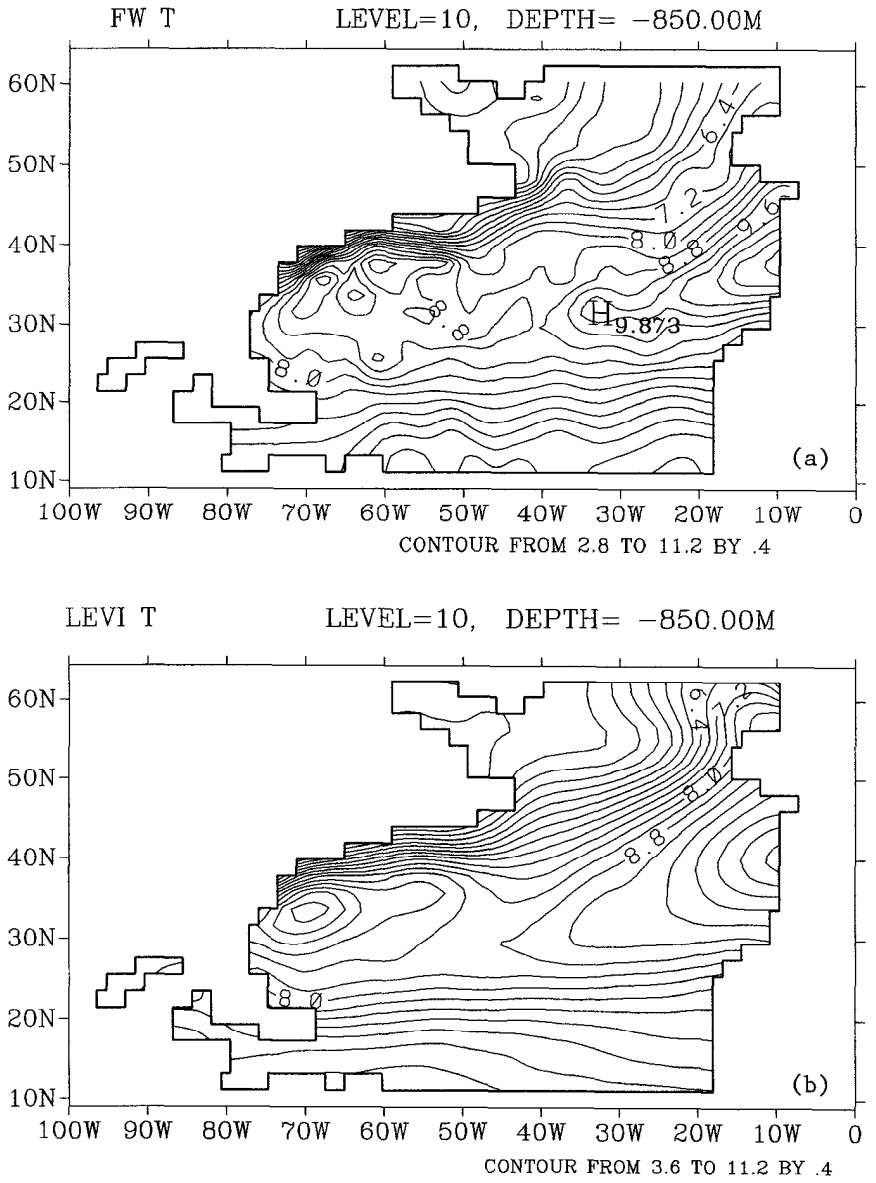

Figure 20. The potential temperature at 850 m. (a) the Fukumori and Wunsch climatology and (b) the Levitus climatology (CI = 0.4°C). Note the difference of these two climatologies at the latitude around 45N.

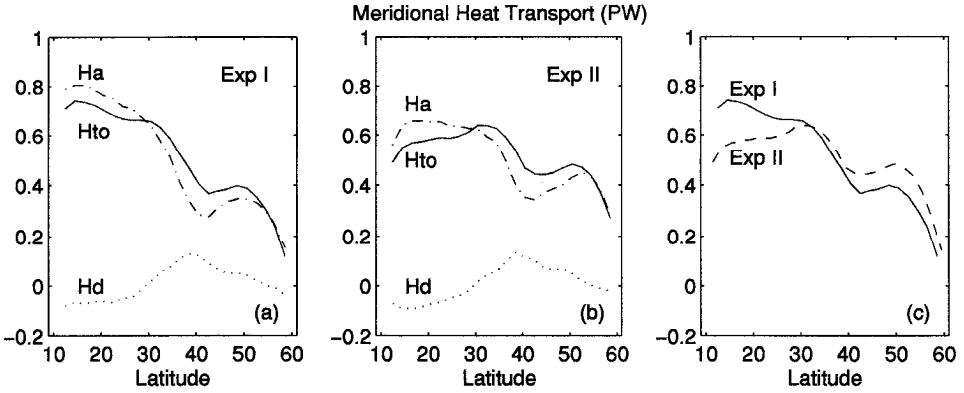

Figure 21. The northward heat transport (Petawatts) obtained from (a) Exp. I and (b) Exp. II (Solid line: total transport; dash-dotted line: advective transport; dotted line: diffusive transport. The comparison between the two experiments is shown in (c).

transports less heat and salt northward and produces locally a cooler and fresher water mass. Considering that the assimilation forces the modeled state close to the climatology, the only way to warm up and salify the local water mass is through the local enhancement of the heat input and the evaporation.

Comparisons between Exp. I and Exp. II. Compared to Exp. I, the fluxes obtained from Exp. II (Fig. 23) have many small structures despite that they have roughly similar large-scale distributions. These small-scale structures (or "noises"), prevailing over the Gulf Stream extension (particularly near 40N) and the Labrador Sea, induce intensive heating/cooling centers in contrast to the surroundings. Schiller (1995) also found in his study that the fluxes obtained from the Levitus hydrography have a large departure from the flux data (the climatological flux he used were calculated from the "Comprehensive Ocean Atmosphere Data Set" with Bunker wind field and bulk coefficients). However, the estimated fluxes from his experiments looked much smoother than this study due to his use of a flux limitation condition in the procedure. This condition, which required that the estimated flux value be equal to the value of three standard deviations whenever the flux deviates larger than that, is rather arbitrary and ignores the physics behind. In the following we are going to discuss the mechanisms responsible for the "noisy" flux estimates. For convenience, only the heat flux is analyzed and the same analysis can be extended to the fresh water flux estimation.

For the upper water column, the following heat budget balance holds at the steady state:

$$Q = c_p \rho h(\mathbf{u} \cdot \nabla_h T + wT_z - K_h \nabla_h^2 T - K_v T_{zz}). \tag{11}$$

That is, the net surface heat flux is the residual of the heat advection and diffusion at the steady state. The plots of each individual term (not shown) display that, in general, the total diffusive heat flux is much smaller than the total advective heat flux and the surface heat

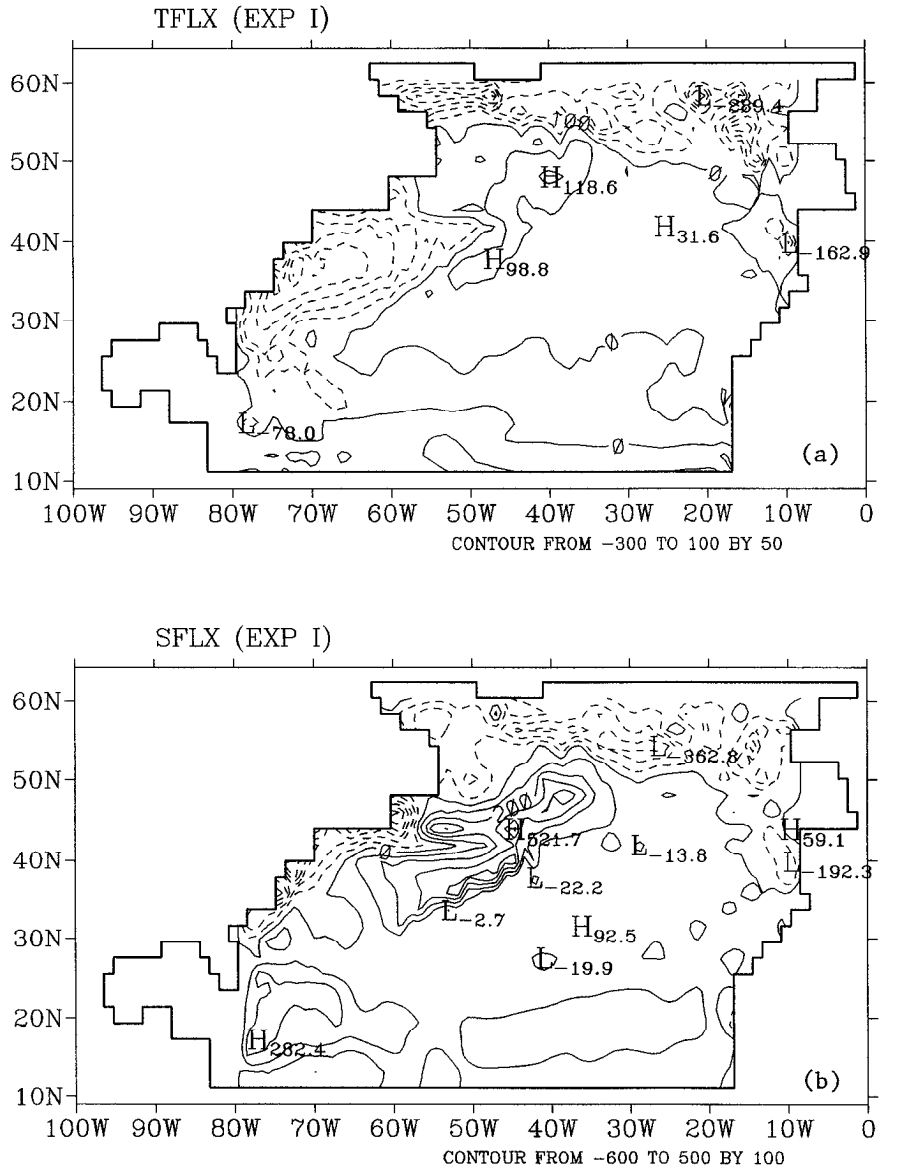

Figure 22. Results from Exp. I (a). The optimal surface heat flux (CI = 50 W/m^2); and (b) the optimal fresh water flux (CI = 100 cm/year).

flux pattern is mainly determined by the heat advection; furthermore, the horizontal heat advection (i.e., $\mathbf{u} \cdot \nabla_h T$) is dominant over the vertical advection. Therefore, the optimal heat flux pattern mainly reflects the pattern of the horizontal heat advection (see Figs. 24 and 25).

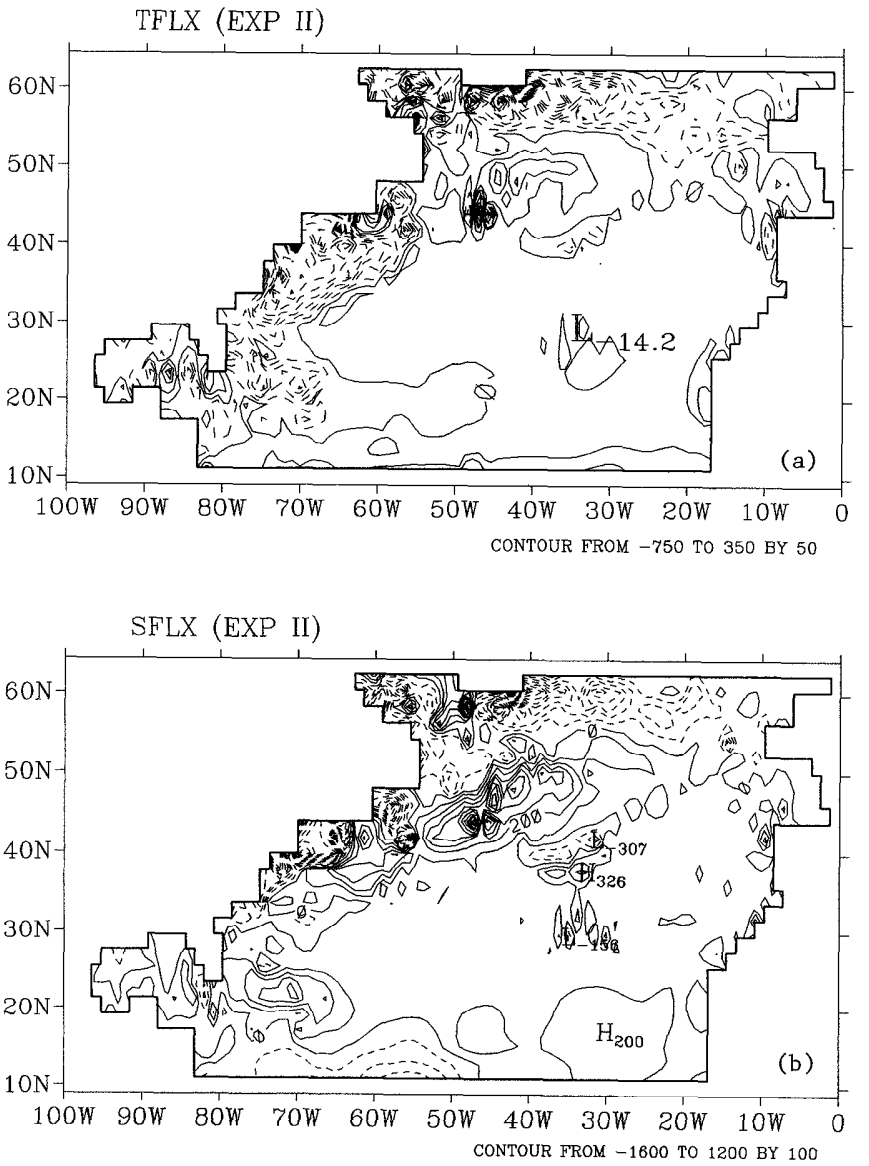

Figure 23. As in Figure 22 but for Exp. II.

The horizontal heat advection, as its mathematical expression indicates, is the inner product of the two vectors **u** and $\nabla_h T$. As a result, the heat advection is minimal if the current runs parallel to the isotherm and is maximal if the current is across the isotherm. Therefore, one anticipates a smooth heat advection pattern, if the angle between the two vectors, **u** and $\nabla_h T$, keeps smooth. As is shown in Figures 22 and 23, Exp. I has a smooth

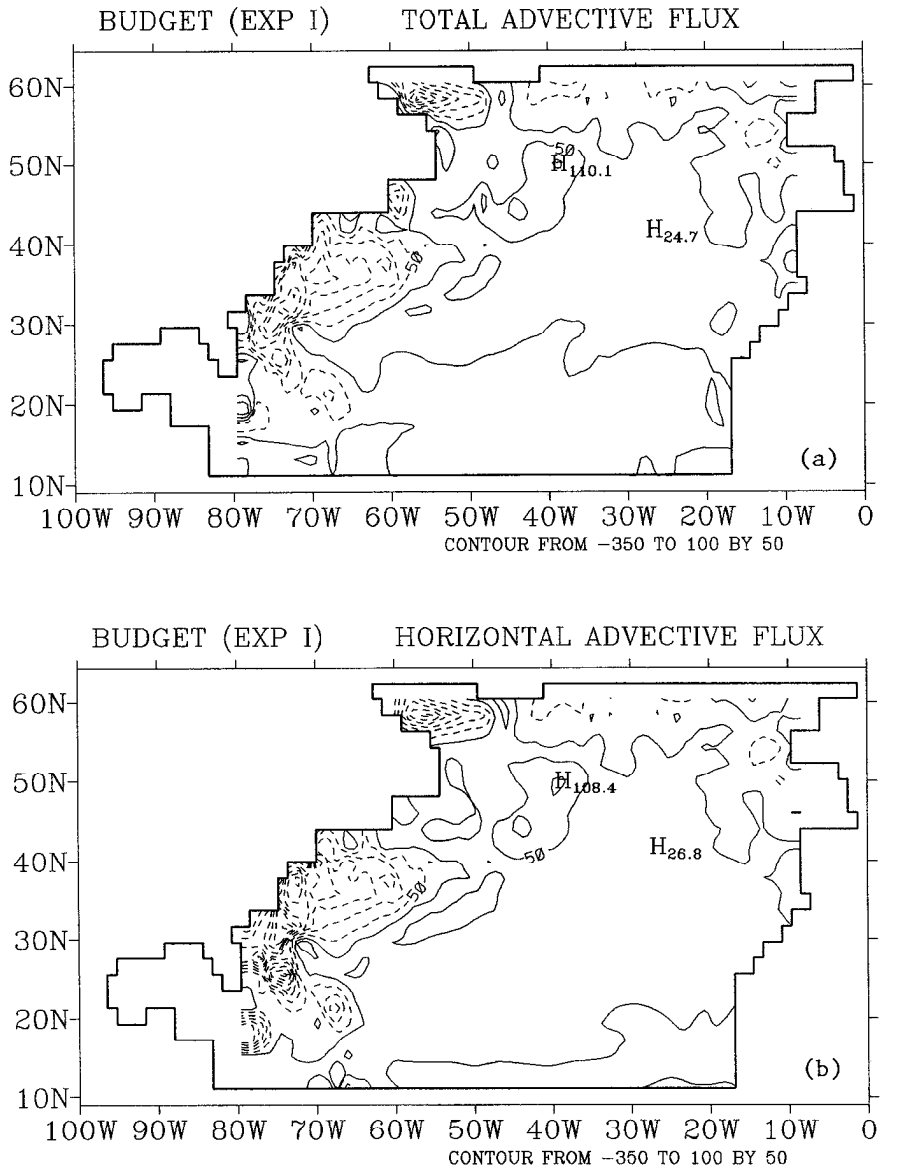

Figure 24. Heat budget analysis for the upper ocean for Exp. I (a) total advective heat flux ($\mathbf{u} \cdot \nabla_h T + wT_Z$;) and (b) horizontal contribution ($\mathbf{u} \cdot \nabla_h T$) (CI = 50 W/m^2 for all plots).

horizontal heat advection pattern in the region of Gulf Stream compared to Exp. II. From the above argument, we can say that the subarctic frontal structure in the FW91 climatology matches better with the current structure. Since the upper ocean circulation is primarily wind-driven and since the same Hellerman-Rosenstein wind forcing field is used

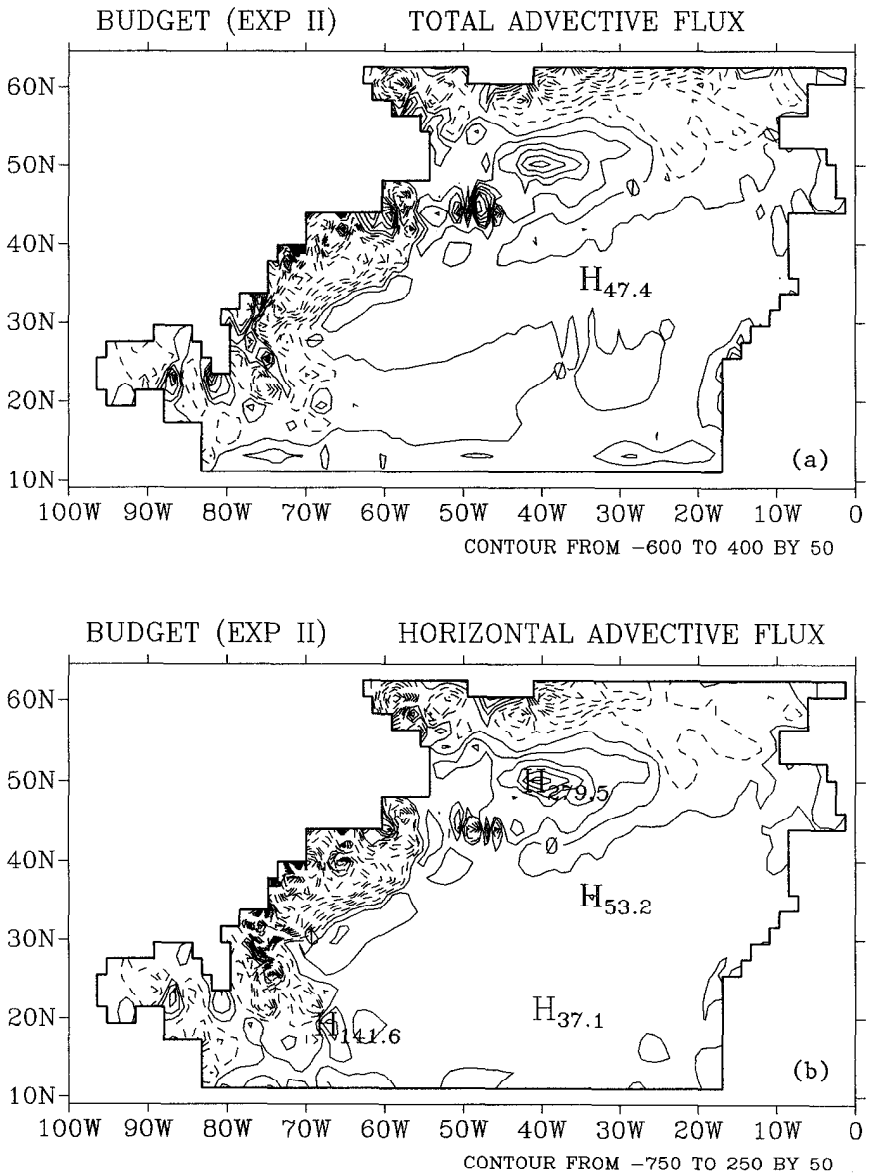

Figure 25. As in Figure 24 but for Exp. II.

for both experiments, we expect that the two experiments simulate a similar circulation pattern in the upper ocean (see Figs. 17 and 18). Thus, the differences between Exp. I and II with regards to the flux distribution must be attributable to the differences of the two climatological hydrographies.

One possible explanation for the noisy flux estimations is as follows. The study of Lozier *et al.* (1994) reveals that the Levitus averaging procedure creates anomalous potential temperatures dissimilar to the surrounding water. This point can be understood by examining the two SST climatologies shown in Figure 4. The isotherm curvature structure associated with the Gulf Stream is clearly evident in the FW91 hydrography, but virtually absent in the Levitus hydrography; the latter hydrography looks more like a smoothed version of the former. Obviously smoothing an uneven curve would leave behind small-scale structures, which, in the case of the Levitus climatology, can result in temperature anomalies. In the assimilation, these anomalies destroy the structure congruence between the temperature and current fields and lead to inconstant crossings between $\mathbf{u}$ and $\nabla_h T$—this produces the anomalies of the heat advection. In addition, the imposed model-data constraints maintains the localization of these anomalous heat advections and therefore, anomalous changes are introduced to the surface heat flux.

Comparisons between Exp. I and II clearly demonstrate the importance of data quality in controlling the quality of the optimal flux estimation. The dynamical model plays an important role in the adjoint calculation because it induces physical adjustments to orient the model state close to data. The adjustments might be unrealistic (or anomalous) if data are noise-contaminated.

c. Results from Exps. III and IV

Table 1 illustrates that the structural difference between Exps. I/II and Exps. III/IV is the cost function, while in the latter the cost formulation includes additional constraints for the flux estimation. The added flux constraints penalize the departure of the estimated surface heat and fresh water fluxes from the Oberhuber climatological fluxes. By doing so, the minimization searches an optimal estimate of the surface fluxes and the model initial states in a way that not only the model state is steady and consistent with the hydrographic climatology, but also the estimated surface fluxes are close to the flux climatology.

The analysis in Section 4a has indicated that Exp. IV does not satisfy the global requirement for a minimum. This is based on the fact that, at the end of the assimilation, the two flux cost values are dominant over the rest of the terms and constitute more than half of the total cost (Table 2). It seems that the current procedure is not successful in finding an optimal solution which is consistent with both the Levitus hydrographic climatology and the Oberhuber flux climatology, even re-starting the procedure with different first guess field. Compared to Exp. IV, the model steady state obtained from Exp. III agrees well with both the FW91 hydrography and the Oberhuber fluxes. In addition, the flux constraints have minor effect on the values of other cost terms of comparing Exp. III with Exp. I, yet they cause large temporal drifts in Exp. IV.

Figure 26 and 27 show the surface heat fluxes obtained from Exps. III/IV and their departures from Oberhuber heat flux. By comparing Figures 22 and 23, one observes that the heat flux patterns from Exps. III/IV closely resemble those from Exps. I/II in all

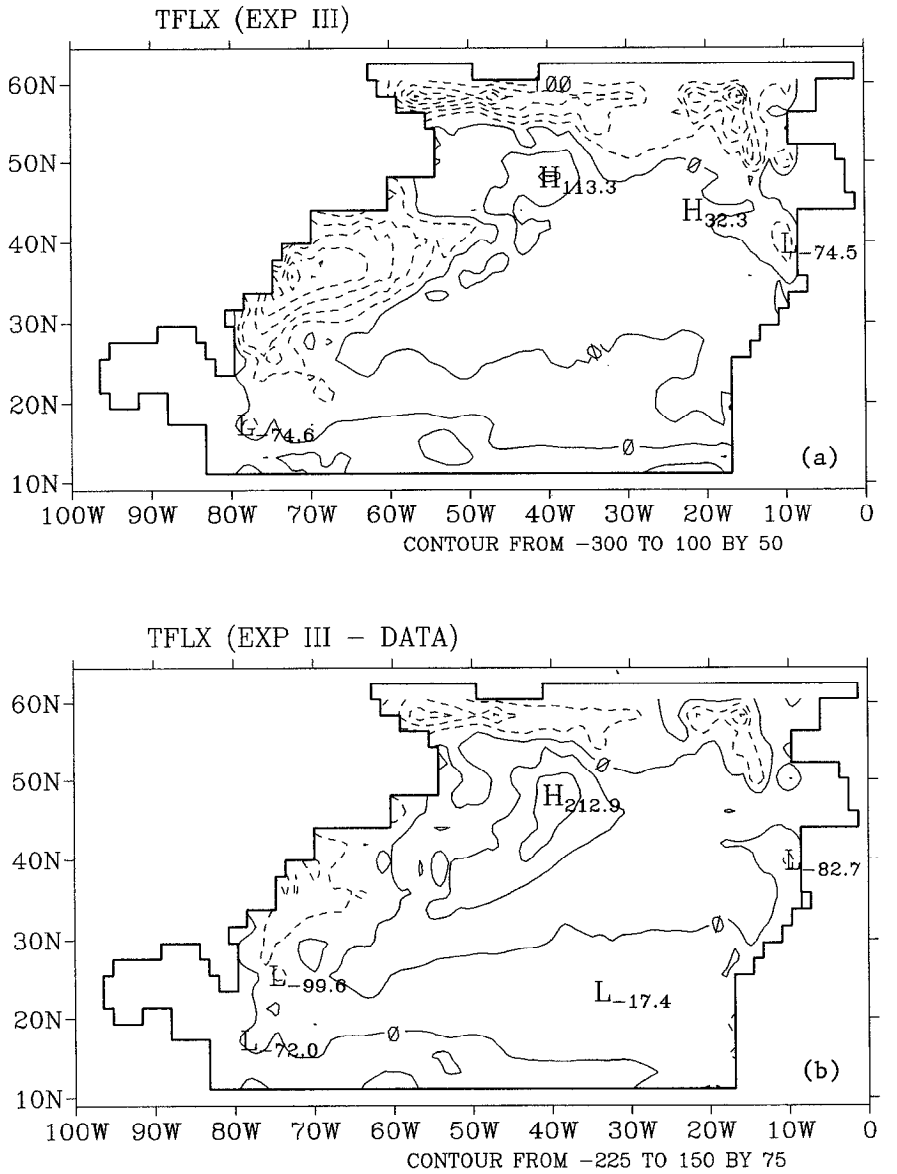

Figure 26. Results from Exp. III. (a) the optimal surface heat flux (CI = 50 W/m^2); and (b) the flux data residuals (difference between the optimal heat flux and the Oberhuber heat flux) (CI = 75 W/m^2).

large-scale aspects. The only difference between the two sets of heat flux patterns is that the fluxes from Exps. III/IV have a smoother spatial distribution and many of the small-scale structures shown in Exps. I/II have been left out. It seems that the flux constraints function as a "filter" during the assimilation and they represent a modifier to the flux pattern

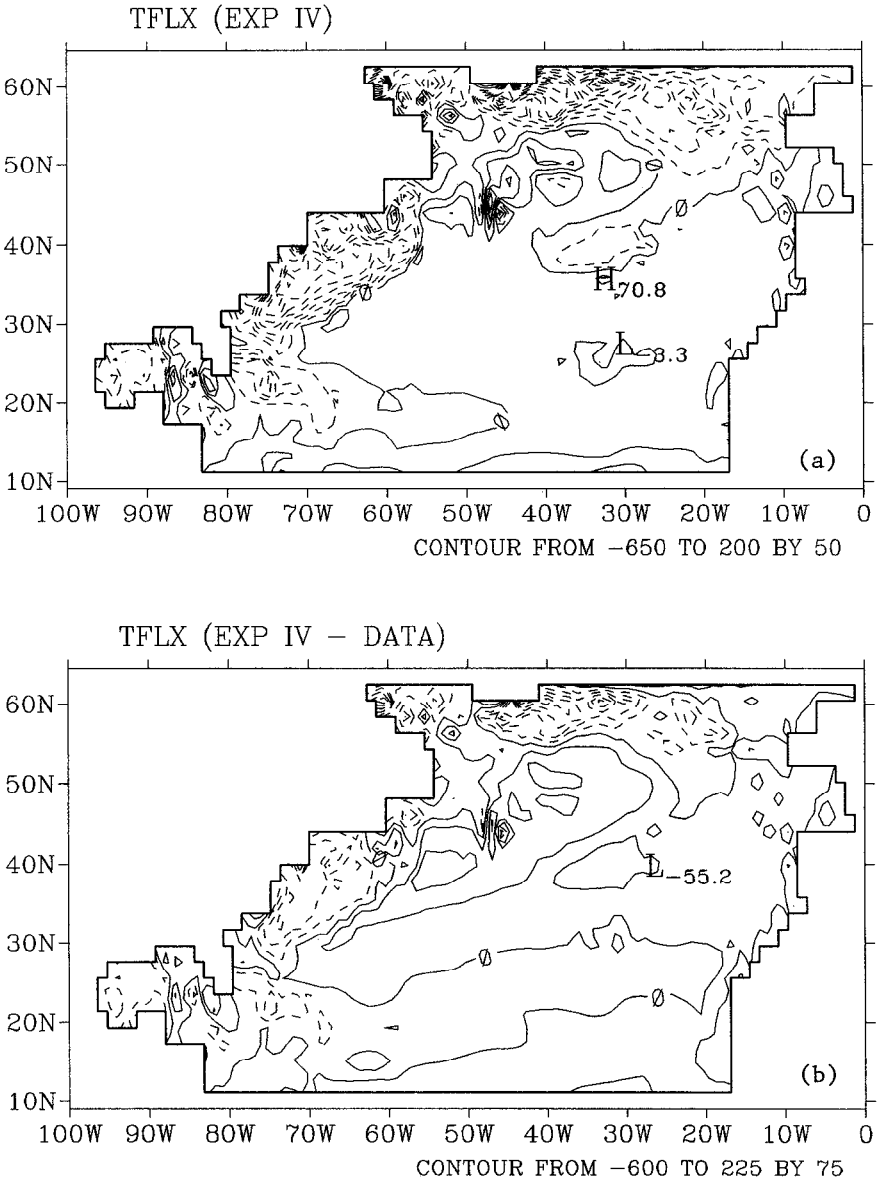

Figure 27. As in Figure 26 but for Exp. IV.

estimated from only the hydrography. The optimal surface fresh water fluxes (not shown) from Exps. III/IV also show the smoothing character of the flux constraints.

In the adjoint procedure, the new estimates of the surface fluxes are computed through the use of other gradient information of the cost function. The gradient of the cost function

(1) with respect to the surface fluxes is,

$$g_{mij} = W^{Qm}(Q_{mij} - \hat{Q}_{mij}) - \sum_{n=1}^{N_T} \lambda_{mij} \qquad \text{where } m = T, S. \tag{12}$$

The first term is the gradient of the flux constraint and the second is the coupling to the model dynamics through the Lagrange multipliers. For Exps. I and II, the gradient, g_{mij}, has only the second component. As is known, the Lagrange multipliers are computed from the adjoint equation (see Eq. 7) and therefore, the second term in (12) is dynamically active; the search along its direction will lead to a model steady state close to the climatological hydrography. On the other hand, the first term represents an imposed direction that guides the estimated surface fluxes toward climatological flux. If climatological flux and hydrography are not dynamically consistent with the steady state assumption, the two directions will not be the same. If this is the case, the minimization, searching along the direction g_{mij}, is only able to achieve a compromise among the data, steadiness and flux constraints. Since the climatological map (Fig. 3) is very smooth, much smoother flux estimates result.

The noise level of the Oberhuber heat flux is assumed to be 75 W/m^2 which includes errors brought by measurement and sampling, errors introduced by data processing schemes and model errors. The plots of the flux data residuals (Figs. 26b, 27b) indicate, though a large noise level is specified, the fit of the estimated flux to climatology is generally quite poor in Exp IV. The estimated flux has a large departure from the climatology in regions of the Gulf Stream and along the northern boundary. On the other hand, the flux from Exp. III agrees in general with the Oberhuber map within the assumed error level, except in regions east of Newfoundland and near the northern boundary where the misfits exceed two standard deviations.

The meridional volume transport stream functions (Fig. 28) show a great similarity to the structures produced by Exp. I/II. The only noticeable difference is that there is a slight increase in the strength of the NADW cell, especially in Exp. IV. This is induced by the stronger surface heat release near the northern boundary in Exps. III/IV (Figs. 26 and 27). Also shown in Figure 28 is the plot of other meridional heat transport from all the four experiments. Obviously, the weaker northward heat transports of Exps. III/IV result from their weaker surface heat fluxes. The relative larger difference between Exps. II and IV shows that the degree of smoothness induced by the heat flux constraint is larger in Exp. IV than in Exp. III.

Examining the temperature residual fields (Figs. 29 and 30), one can see that, though adding the flux constraints does not have much impact on the data residual fields, it produces a larger temporal drift compared to Exps. I/II. The magnitude of the magnified drift is proportional to the degree of the smoothness induced by the heat flux constraint. Clearly the drift in Exp. IV is much larger than in Exp. III. The misfit exceeding two standard deviations appears only in a few one-grid points in Exp. III, but they appear over a large area in Exp. IV.

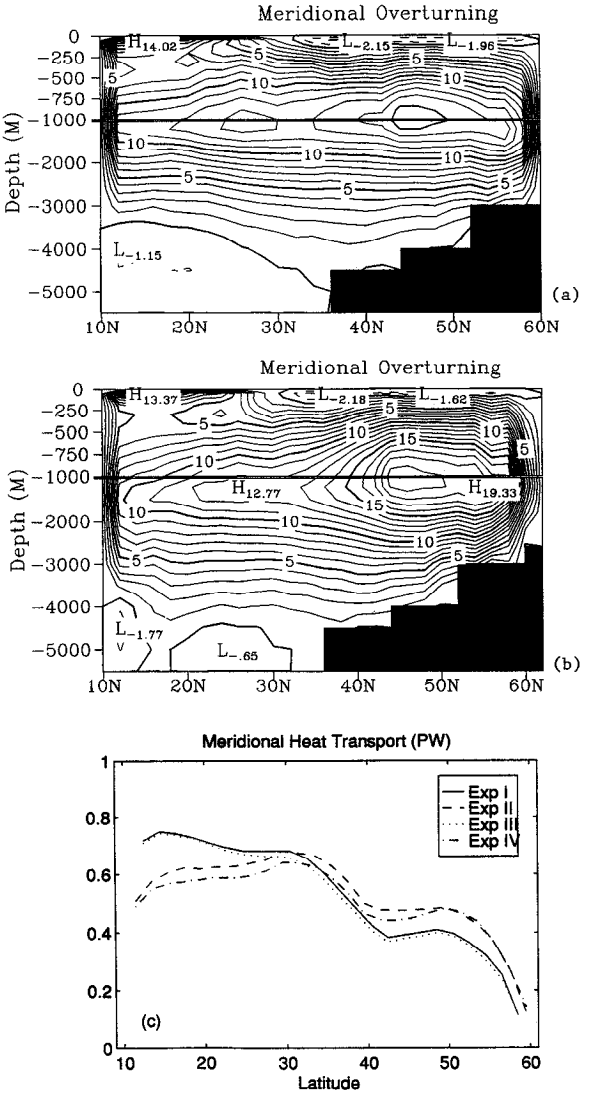

Figure 28. The meridional transport stream function (Sv) obtained from (a) Exp. III; and (b) Exp. IV (CI = 1 Sv). (c) The meridional heat transport (Petawatts) from all the four experiments.

5. Conclusions

The study has presented results of using an exact adjoint of the full Bryan-Cox primitive equation model for inverse modeling of the oceanic general circulation in the North Atlantic. The three issues specified in the Introduction are examined in four experiments, by using the climatological hydrographies from Levitus (1982) and from Fukumori and Wunsch (1991) and/or the Oberhuber (1988) climatological fluxes. The model input

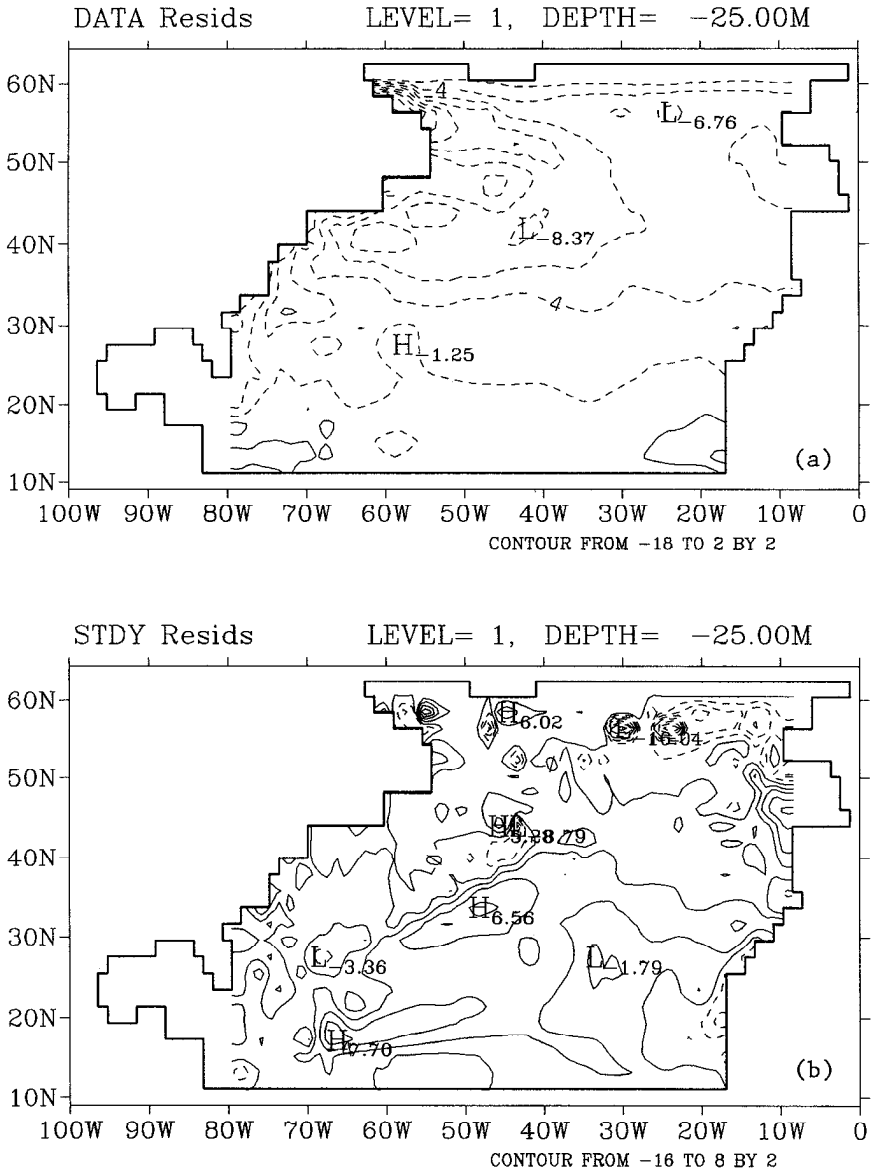

Figure 29. Results from Exp. III. (a) the SST data residuals; and (b) the SST steadiness residual (CI = 2°C).

parameters (the air-sea fluxes of heat and fresh water, and model initial states) are determined through searching a steady state circulation consistent with the climatologies.

The study has shown that the optimized temperature field has a basin-wide cold surface layer, a feature that has been reported by all studies of North Atlantic general circulation

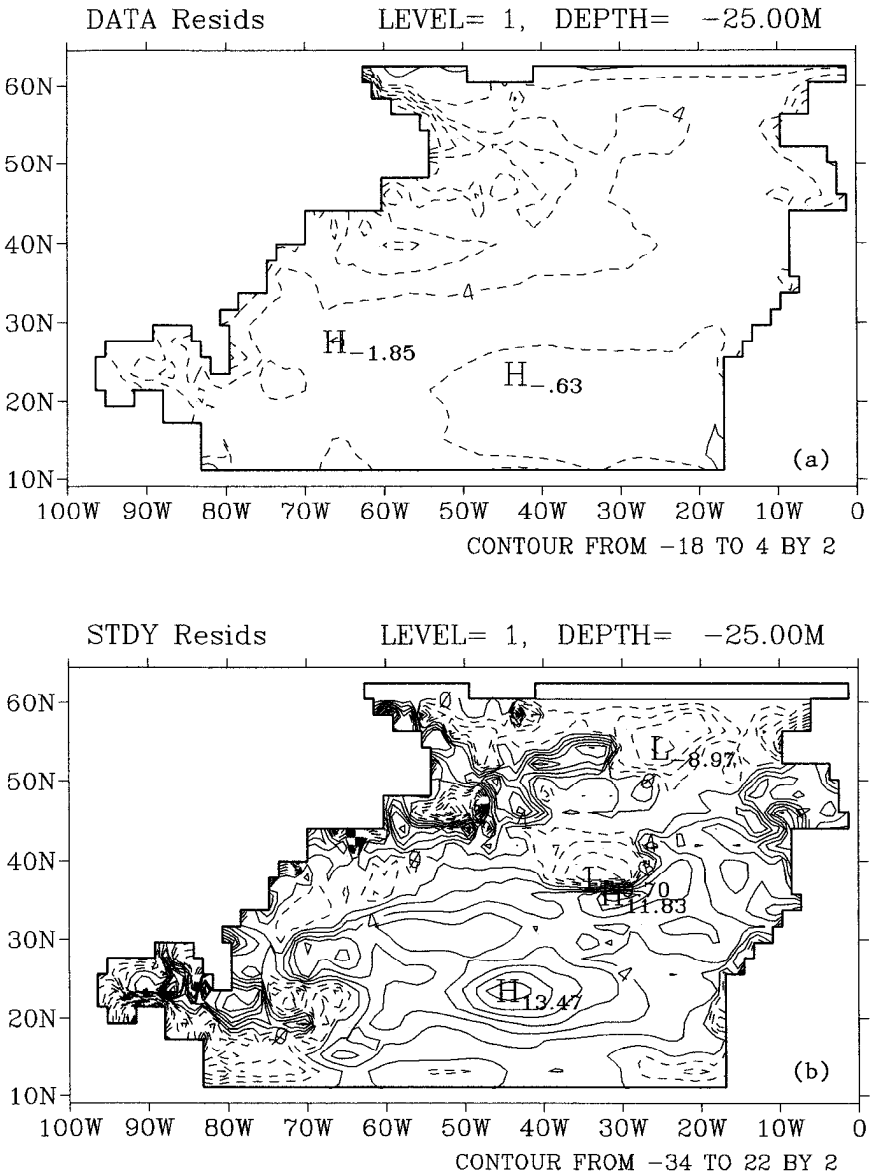

Figure 30. As in Figure 29 but for Exp. IV.

with inverse OGCMs (Tziperman *et al.*, 1992b; Marotzke and Wunsch, 1993; and Schiller, 1995). However, our study has found that this surface cold bias reflects just part of the systematic error pattern in the vertical—*the model has a warm bias in the deep ocean.* We believe that the cold surface layer is a correction imposed by the optimization to reduce large data misfits in the deep ocean due to the deep warming. This deep warming results

from the combined effects of using the steady state assumption, the annual mean climatology and the relaxation boundary condition at the model's northern boundary. The annual mean hydrography has a surface water warmer than the observed winter surface water, and a deep ocean whose properties are determined by the winter surface water at high latitudes. Due to the imposed relaxation condition at the model's northern boundary, deep waters are formed through the artificial sinking of surface waters with annual-mean temperatures in the relaxation zone. This process leads to a warm deep ocean and large model-data discrepancies in the vast deep layer. In order to reduce the misfits as required by the optimal procedure, the surface layer which is the source for the modeled deep water needs to be cooler. The strong and deep vertical mixing formed in the model provides the means for an effective cooling. The results have further shown that the degree of the surface correction depends on how much of the surface cooling is necessary to minimize the overall data misfits. The surface cooling is stronger when assimilating the FW91 hydrography (Exp. I), because this climatology was compiled from the summer-dominated data source and has a consequent warmer surface water. The study suggests that a better simulation of the 3-D hydrography requires at least the inclusion of seasonal forcings, and we are in the process of assimilating the seasonal climatological data.

Moreover, the study has identified a problem in the Levitus climatology. In using it for the assimilation, Exp. II obtains two anomalous features, one is a strong zonally integrated upwelling in the midlatitude North Atlantic and the other a very noisy flux estimation. The analysis indicates that both features are related to the smeared Gulf Stream frontal structure of the Levitus hydrography. The upwelling is induced by the exaggerated *horizontal advective flux* of heat that is balanced by the vertical advection rather than by the cross-frontal diffusion as is the "Veronis effect." The noisy flux estimation, as a possible hypothesis indicates that the isotherms and the streamlines are not parallel; inconstant crossings between $\mathbf{u}$ and $\nabla_h T$ create anomalies of the heat/salt advection, which in turn induce the corresponding anomalous changes in the surface heat/fresh water flux fields. This suggests that high quality observations are a prerequisite for quality data assimilation.

The dynamical coupling between the climatological hydrography and fluxes (the second objective) is studied. Table 2 shows that the experiments, except Exp. IV, have produced a cost value which satisfies the global measure of a minimum. However, the analysis of residual fields reveals that some systematic discrepancies exist between the modeled and the climatological hydrographies, such as the overall underestimation of upper ocean temperatures and overestimation of deep water temperatures, and the under-representation of the Mediterranean salt tongue. Although, on the average, the magnitudes of the residuals are within the preassumed error estimates, the patterns show a correlated error structure. The assumption of using a diagonal weighting matrix in the cost function (1) is not satisfied. The experiments, however, illustrate that, within the dynamical framework of the steady state solution, the FW91 hydrography is dynamically more compatible with the Oberhuber climatological fluxes compared with the Levitus hydrography. This is clearly

demonstrated in Exp. IV, in which the flux penalty induces a large temporal drift in the model and makes the optimization procedure unable to find a steady solution.

Finally, the impact of the model on the propagation of the data information (the third objective) is analyzed. The results show that the full OGCM dynamics substantially help the model in better simulating the frontal structures of the Gulf Stream system. Additionally the large-scale features in the velocity fields are much less noisier than those in the study of Marotzke and Wunsch (1993), demonstrating the advantage of the full OGCM and its adjoint over simplified OGCMs and/or adjoints. However, the model suffers from an adequate representation of the North Atlantic Current and the Mediterranean salt tongue; the former is due to the limitation of the model domain and the latter is caused by the lack of the physical condition of the Mediterranean outflow. These model errors can induce an erroneous correction in the assimilation. As is shown in the analysis of the estimated surface fluxes, the anomalous heating and high evaporation center off Newfoundland is directly linked to the weak North Atlantic Current.

In conclusion, the study has shown the promise of success in using the combined OGCM/adjoint model for the large-scale data assimilation. A further goal we envision with this model is to exploit real-time observations in constructing the four-dimensional pictures of the ocean general circulation.

Acknowledgments. Andrea Bergamasco is acknowledged for his assistance in the initial set-up of the base code of the adjoint OGCM and for technical help. Jochem Marotzke is thanked for his suggestions and comments during the reconstruction of the adjoint OGCM and for reviewing the first draft of the manuscript. Constructive comments on the manuscript from Eli Tziperman are sincerely appreciated. The computations were conducted on the Cray-YMP at the National Center for Atmospheric Research and on the Cray-C98 at the NASA Goddard Space Flight Center. This research was carried out with the support of the National Aeronautics and Space Administration, Grant no. NAGW-2711 (P. Malanotte-Rizzoli and L. Yu).

APPENDIX

The essential assumptions of the model are the hydrostatic assumption, the Bossinesq approximation, and a closure approximation for small-scale motions based on the turbulent viscosity hypothesis. The momentum and continuity equations are

$$\mathbf{u}_t + \mathbf{u} \cdot \nabla_h \mathbf{u} + w\mathbf{u}_z + f\mathbf{k} \times \mathbf{u} = -\frac{1}{\rho_o}\nabla_h p + A_v \mathbf{u}_{zz} + A_h \nabla_h^2 \mathbf{u} \tag{A1}$$

$$p_z + \rho g = 0 \tag{A2}$$

$$\nabla_h \cdot \mathbf{u} + w_z = 0 \tag{A3}$$

where $\mathbf{u}$ is the horizontal velocity vector with components (u, v) in the zonal (λ) and meridional (ϕ) directions, and w the vertical velocity; p, ρ, g, and f are pressure, density, the acceleration of gravity, and the Coriolis parameter; $\mathbf{k}$ is a unit vector in the vertical (z)

direction and ∇_h the horizontal gradient operator in spherical coordinates; A_v and A_h the vertical and horizontal eddy viscosity coefficients.

The conservation equations for the potential temperature (T) and salinity (S) under conditions of stable stratification are

$$(T, S)_t + \mathbf{u} \cdot \nabla_h(T, S) + w(T, S)_z = K_v(T, S)_{zz} + K_h\nabla_h^2(T, S) \tag{A4}$$

where K_v and K_h are the vertical and horizontal diffusivities of heat and salt. In case the model predicts a gravitational instability, the conventional convective adjustment scheme is employed so that the water column is mixed vertically until stability is restored.

The equation of state relating density to potential temperature, salinity, and pressure is complicated, but can be computed by a polynomial approximation whose coefficients are fitted to the standard Knudsen formula (Bryan and Cox, 1972). In general

$$\rho = \rho(T, S, p) \tag{A5}$$

The boundary conditions are specified as follows. At the sidewalls of the basin,

$$\mathbf{u} \cdot \mathbf{n} = 0 \tag{A6}$$

$$\mathbf{n} \cdot [K_h\nabla_h(T, S)] = 0 \tag{A7}$$

where $\mathbf{n}$ denotes a unit vector normal to the wall.

At the ocean bottom

$$w = -\mathbf{u} \cdot \nabla_h H \tag{A8}$$

$$A_v\mathbf{u}_z = 0 \tag{A9}$$

$$K_v(T, S)_z = 0 \tag{A10}$$

At the surface

$$w = 0 \tag{A11}$$

$$A_v\mathbf{u}_z = \tau/\rho_a \tag{A12}$$

$$K_v(T, S)_z = (Q_T, S_0Q_S) \tag{A13}$$

where τ is the wind stress vector with components (τ^x, τ^y). The surface thermal and saline boundary conditions take the form of specified fluxes of heat Q_T and fresh water Q_S. They are the parameters to be determined from the adjoint calculations along with the initial model states.

The numerical implementation of (A1)–(A13) follows the method described in Bryan (1969) and in Cox (1984). The integration of the hydrostatic relation (2) yields

$$p = p_s + \int_z^0 \rho g dz. \tag{A14}$$

No prognostic equation for the pressure p_s at $z = 0$ is available and p_s must be eliminated from the equations. This can be done by first decomposing the velocities in the form

$$\mathbf{u} = \mathbf{U} + \hat{\mathbf{u}} \tag{A15}$$

where $\mathbf{U} = (1/H) \int_{-H}^{0} \mathbf{u} dz$ and $\hat{\mathbf{u}}$ denote the barotropic and baroclinic components of motion, respectively. If we neglect the part of the pressure gradient force which depends on the surface pressure in the equations (A1) and compute the corresponding velocities $\mathbf{u}'$ based on the following equations

$$\mathbf{u}_t' + \mathbf{u} \cdot \nabla_h \mathbf{u} + w\mathbf{u}_z + f\mathrm{k} \times \mathbf{u} = -\frac{g}{\rho_0}\left(\int_z^0 (\nabla_h \rho)\, dz\right) + A_v \mathbf{u}_{zz} + A_h \nabla_h^2 \mathbf{u} \tag{A16}$$

we can then determine the baroclinic velocities $\hat{\mathbf{u}}$ by

$$\hat{\mathbf{u}} = \mathbf{u}' - \overline{\mathbf{u}'}. \tag{A17}$$

The barotropic velocities are solved through the relation

$$\nabla_h \psi = -\mathbf{k} \times (H\mathbf{U}) \tag{A18}$$

where ψ is the barotropic streamfunction and satisfies the equation

$$\left(\frac{\psi_x}{H}\right)_{xt} + \left(\frac{\psi_y}{H}\right)_{yt} = -J\left(\psi, \frac{f}{H}\right) + \nabla_h \cdot \left\{\frac{1}{H}\int_{-H}^{0}\left[\frac{g}{\rho_0}\int_z^0 (\mathbf{k} \times \nabla_h \rho)\, dz'\right] dz\right\} + \nabla_h \cdot \left(\frac{1}{H}\int_{-H}^{0} \mathbf{k} \times \mathbf{G}^{\mathbf{u}}\, dz\right) \tag{A19}$$

where J is the Jacobian operator and $\mathbf{G}^{\mathbf{u}} = \mathbf{u} \cdot \nabla_h \mathbf{u} + w\mathbf{u}_z - A_v \mathbf{u}_{zz} - A_h \nabla_h^2 \mathbf{u}$. The total velocities are obtained form (A15) and are then used to predict the temperature and salinity equations (A4).

For the sake of convenience in the discussion, the discretized form for the above equations are generalized as

$$\mathscr{X}_{ijk}^{n} = \mathscr{F}_n(\mathscr{X}_{ijk}^{n-1}, Q_{Tij}, Q_{Sij}) \qquad n = 1, 2, \ldots, N_T \tag{A20}$$

where (ijk) is the grid location, $\mathscr{X}_{ijk}^{n} = (\mathbf{u}_{ijk}^n, T_{ijk}^n, S_{ijk}^n, \psi_{ijk}^n)^T$ a vector of the model prognostic variables at time step n, and $(\ )^T$ means transpose. The total integration time is denoted as N_T.

REFERENCES

Bergamasco, A., P. Malanotte-Rizzoli, W. C. Thacker and R. B. Long. 1993. The seasonal steady circulation of the Eastern Mediterranean determined with the adjoint method. Deep-Sea Res. II, *40,* 1269–1294.

Böning, C. W., W. R. Holland, F. O. Bryan, G. Danabasoglu and J. C. McWilliams. 1995. An overlooked problem in model simulations of the thermohaline circulation and heat transport in the Atlantic Ocean. J. Climate, *8,* 515–523.

Bryan, K. 1969. A numerical method for the study of the circulation of the world ocean. J. Comp. Phys., *4,* 347–376.

Bryan, K. and M. D. Cox. 1972. An approximate equation of state for numerical models of the ocean circulation. J. Phys. Oceanogr., *2,* 510–514.

Cox, M. D. 1984. A primitive equation, three-dimensional model of the ocean. GFDL Ocean Group Tech. Rep. 1, Geophys. Fluids Dyn. Lab., Princeton, NJ, 137 pp.

Fukumori, I., F. Martel and C. Wunsch. 1991. The hydrography of the North Atlantic in the early 1980s. An Atlas. Prog. Oceanogr., *27,* 1–110.

Fukumori, I. and C. Wunsch. 1991. Efficient representation of the North Atlantic hydrographic and chemical distributions. Prog. Oceanogr., *27,* 111–195.

Hall, M. M. and H. L. Bryden. 1982. Direct estimates and mechanisms of ocean heat transport. Deep-Sea Res., *29,* 339–360.

Han, Y. J. 1984. A numerical World Ocean general circulation model. Part II. A baroclinic experiment. Dyn. Atmos. Oceans, *8,* 141–172.

Hellerman, S. and M. Rosenstein. 1983. Normal monthly wind stress over the world ocean with error estimates. J. Phys. Oceanogr., *13,* 1093–1104.

Holland, W. R. and F. O. Bryan. 1993. Senstivitiy studies on the role of the ocean in climate change, *in* Ocean Processes in Climate Dynamics: Global and Mediterranean Examples. P. Malanotte-Rizzoli and A. R. Robinson, eds., Kluwer, 111–134.

Le Dimet, F. and O. Talagrand. 1986. Variational algorithm for analysis and assimilation of meteorological observations: theoretical aspects. Tellus, *38A,* 97–110.

Levitus, S. 1982. Climatological atlas of the world ocean. NOAA Tech. Paper, 173 pp.

Long, R. B., S. M. Hwang and W. C. Thacker. 1989. The finite-difference equations defining the GFDL-GCM and its adjoint. Unpublished report. Atlantic Oceanographic and Meterological Laboratory, Miami, Florida.

Lozier, M. S., M. S. McCartney and W. B. Owens. 1994. Anamalous anomalies in averaged hydrographic data. J. Phys. Oceanogr., *24,* 2624–2638.

Marotzke, J. 1992. The role of integration time in determining a steady state through data assimilation. J. Phys. Oceanogr., *22,* 1556–1567.

Marotzke, J. and C. Wunsch. 1993. Finding the steady state of a general circulation model through data assimilation: Application to the North Atlantic ocean. J. Geophys. Res., *98,* 20,149–20,167.

Navon, I. M. and D. Legler. 1987. Conjugate-gradient methods for large-scale minimization in meteorology. Mon. Wea. Rev., *115,* 1479–1502.

Oberhuber, J. M. 1988. An atlas based on the COADS data set: the budgets of heat, buoyancy and turbulent kinetic energy at the surface of the global ocean. Max-Plank-Institut Für Meteorologie, Hamburg, Germany, 100 pp.

Sasaki, Y. 1970. Some formulations in numerical variational analysis. Mon. Wea. Rev., *98,* 875–883.

Schiller, A. 1995. The mean circulation of the Atlantic Ocean north of 30S determined by the adjoint method. J. Mar. Res., *53,* 453–497.

Schiller, A. and J. Willebrand. 1995. A technique for the determination of surface heat and freshwater fluxes from hydrographic observations using an approximate adjoint ocean circulation model. J. Mar. Res., *53,* 433–451.

Sirkes, Z. and E. Tziperman. 1995. Combining data and a global primitive equation ocean general circulation model using the adjoint method, *in* Modern Approaches to Data Assimilation in Ocean Modeling, P. Malanotte-Rizzoli, ed., Elsevier Science, 119–145.

Thacker, W. C. and R. B. Long. 1988. Fitting dynamics to data. J. Geophys. Res., *93,* 1227–1240.

Tziperman, E. and K. Bryan. 1993. Estimating global air-sea fluxes from surface properties and from climatological flux data using an oceanic GCM. J. Geophys. Res., *98,* 22,629–22,644.

Tziperman, E. and W. C. Thacker. 1989. An optimal control/adjoint equations approach to studying the oceanic general circulation. J. Phys. Oceanogr., *19,* 1471–1485.

Tziperman, E., W. C. Thacker, R. B. Long and S. Hwang. 1992a. Oceanic data analysis using a general circulation model. Part I. Simulations. J. Phys. Oceanogr., *22,* 1434–1457.

Tziperman, E., W. C. Thacker, R. B. Long, S. Hwang and S. R. Rintoul. 1992b. Oceanic data analysis using a general circulation model. Part II. A North Atlantic model. J. Phys. Oceanogr., *22,* 1458–1485.

Veronis, G. 1975. The role of models in tracer studies, *in* Numerical Models of the Ocean Circulation, National Academy of Sciences, 133–146.

Weare, B. C., P. T. Strub and M. D. Samuel. 1981. Annual mean surface heat fluxes in the tropical Pacific Ocean. J. Phys. Oceanogr., *11,* 705–717.

Yu, L. and P. Malanotte-Rizzoli. 1995. Assimilation of North Atlantic climatologies using a primitive equation model—Sensitivity studies, *in* Proceedings of Second International Symposium on Assimilation of Observations in Meterology and Oceanography, Tokyo, Japan. Vol. II, 565–570.

Received: *24 October, 1995;* revised: *30 May, 1996.*